



Calhoun: The NPS Institutional Archive
DSpace Repository

Theses and Dissertations

1. Thesis and Dissertation Collection, all items

2014-06

Finite element and analytical analysis of cracks in thick stiffened plates repaired with a singlesided composite patch

Hall, Benjamin L.

Monterey, California: Naval Postgraduate School

<http://hdl.handle.net/10945/42638>

This publication is a work of the U.S. Government as defined in Title 17, United States Code, Section 101. Copyright protection is not available for this work in the United States.

Downloaded from NPS Archive: Calhoun



Calhoun is the Naval Postgraduate School's public access digital repository for research materials and institutional publications created by the NPS community. Calhoun is named for Professor of Mathematics Guy K. Calhoun, NPS's first appointed -- and published -- scholarly author.

Dudley Knox Library / Naval Postgraduate School
411 Dyer Road / 1 University Circle
Monterey, California USA 93943

<http://www.nps.edu/library>



NAVAL POSTGRADUATE SCHOOL

MONTEREY, CALIFORNIA

THESIS

**FINITE ELEMENT AND ANALYTICAL ANALYSIS OF
CRACKS IN THICK STIFFENED PLATES REPAIRED
WITH A SINGLE-SIDED COMPOSITE PATCH**

by

Benjamin L. Hall

June 2014

Thesis Advisor:
Second Reader:

Young W. Kwon
Jarema M. Didoszak

Approved for public release; distribution is unlimited

THIS PAGE INTENTIONALLY LEFT BLANK

REPORT DOCUMENTATION PAGE			<i>Form Approved OMB No. 0704-0188</i>	
Public reporting burden for this collection of information is estimated to average 1 hour per response, including the time for reviewing instruction, searching existing data sources, gathering and maintaining the data needed, and completing and reviewing the collection of information. Send comments regarding this burden estimate or any other aspect of this collection of information, including suggestions for reducing this burden, to Washington headquarters Services, Directorate for Information Operations and Reports, 1215 Jefferson Davis Highway, Suite 1204, Arlington, VA 22202-4302, and to the Office of Management and Budget, Paperwork Reduction Project (0704-0188) Washington DC 20503.				
1. AGENCY USE ONLY (Leave blank)		2. REPORT DATE June 2014	3. REPORT TYPE AND DATES COVERED Master's Thesis	
4. TITLE AND SUBTITLE FINITE ELEMENT AND ANALYTICAL ANALYSIS OF CRACKS IN THICK STIFFENED PLATES REPAIRED WITH A SINGLE-SIDED COMPOSITE PATCH			5. FUNDING NUMBERS	
6. AUTHOR(S) Benjamin L. Hall				
7. PERFORMING ORGANIZATION NAME(S) AND ADDRESS(ES) Naval Postgraduate School Monterey, CA 93943-5000			8. PERFORMING ORGANIZATION REPORT NUMBER	
9. SPONSORING /MONITORING AGENCY NAME(S) AND ADDRESS(ES) N/A			10. SPONSORING/MONITORING AGENCY REPORT NUMBER	
11. SUPPLEMENTARY NOTES The views expressed in this thesis are those of the author and do not reflect the official policy or position of the Department of Defense or the U.S. Government. IRB Protocol number ____ N/A ____.				
12a. DISTRIBUTION / AVAILABILITY STATEMENT Approved for public release; distribution is unlimited			12b. DISTRIBUTION CODE	
13. ABSTRACT (maximum 200 words) The purpose of this thesis was to investigate crack growth behavior in thick stiffened aluminum plates repaired with a single-sided composite patch. A model was developed using finite element analysis that extracted the mode I strain energy release rate (SERR) with use of the Virtual Crack Closure Technique. The dimensions and spacing of the stiffeners were varied to determine their effect on reducing the SERR. This model was also compared to an unstiffened model and one without a composite patch. A tensile load and a bending moment were both applied to the model for various configurations. These results were then used to develop an analytical model that can be used to predict the effectiveness of a patched surface.				
14. SUBJECT TERMS composite patch, stiffening member, finite element			15. NUMBER OF PAGES 63	
			16. PRICE CODE	
17. SECURITY CLASSIFICATION OF REPORT Unclassified	18. SECURITY CLASSIFICATION OF THIS PAGE Unclassified	19. SECURITY CLASSIFICATION OF ABSTRACT Unclassified	20. LIMITATION OF ABSTRACT UU	

THIS PAGE INTENTIONALLY LEFT BLANK

Approved for public release; distribution is unlimited

**FINITE ELEMENT AND ANALYTICAL ANALYSIS OF CRACKS IN THICK
STIFFENED PLATES REPAIRED WITH A SINGLE-SIDED COMPOSITE
PATCH**

Benjamin L. Hall
Lieutenant, United States Navy
B.S., Worcester Polytechnic Institute, 2007

Submitted in partial fulfillment of the
requirements for the degree of

MASTER OF SCIENCE IN MECHANICAL ENGINEERING

from the

**NAVAL POSTGRADUATE SCHOOL
June 2014**

Author: Benjamin L. Hall

Approved by: Young W. Kwon
Thesis Advisor

Jarema M. Didoszak
Second Reader

Knox T. Millsaps
Chair, Department of Mechanical and Aerospace Engineering

THIS PAGE INTENTIONALLY LEFT BLANK

ABSTRACT

The purpose of this thesis was to investigate crack growth behavior in thick stiffened aluminum plates repaired with a single-sided composite patch. A model was developed using finite element analysis that extracted the mode I strain energy release rate (SERR) with use of the Virtual Crack Closure Technique. The dimensions and spacing of the stiffeners were varied to determine their effect on reducing the SERR. This model was also compared to an unstiffened model and one without a composite patch. A tensile load and a bending moment were both applied to the model for various configurations. These results were then used to develop an analytical model that can be used to predict the effectiveness of a patched surface.

THIS PAGE INTENTIONALLY LEFT BLANK

TABLE OF CONTENTS

I.	INTRODUCTION.....	1
A.	BACKGROUND	1
	1. FFG-7	1
	2. CG-47	2
	3. Aeronautical Industry	2
B.	LITERATURE REVIEW	3
	1. Symmetric vs. Asymmetric Patching	3
	2. Plate Thickness.....	3
	3. Patch Design	4
	4. Residual Stress	5
	5. Stiffening Members.....	7
	6. Analytical Models.....	7
C.	OBJECTIVES	8
II.	FINITE ELEMENT MODEL.....	9
A.	MODEL DESCRIPTION.....	9
B.	MODEL CONSTRUCTION.....	11
	1. Element Selection	12
	2. Linear vs. Nonlinear	13
C.	APPLICABLE THEORIES.....	14
	1. Crack Growth Modeling	14
	2. Virtual Crack Closure Technique	15
III.	ANALYTICAL MODEL.....	19
IV.	RESULTS AND DISCUSSION	25
A.	TENSILE LOAD.....	25
	1. Change in Crack Length	25
	2. Change in Crack Location	28
	3. Change in Stiffener Parameters	30
	4. Change in Neutral Axis	32
	5. Analytical Comparison.....	37
B.	BENDING MOMENT	38
	1. Change in Stiffener Height.....	39
	2. Change in Plate Thickness	41
V.	CONCLUSIONS AND RECOMMENDATIONS.....	43
A.	CONCLUSIONS	43
B.	RECOMMENDATIONS.....	44
	LIST OF REFERENCES.....	45
	INITIAL DISTRIBUTION LIST	47

THIS PAGE INTENTIONALLY LEFT BLANK

LIST OF FIGURES

Figure 1	Typical Longitudinal Stress Distribution, from [16]	6
Figure 2	Model Geometry	9
Figure 3	Stiffening Member Dimensions	10
Figure 4	Boundary and Load Conditions	11
Figure 5	Alignment of Degrees of Freedom	12
Figure 6	Three Modes of Fracture.....	15
Figure 7	VCCT for Two-dimensional Element, from [6]	16
Figure 8	VCCT for Three-dimensional Elements, from [20].....	17
Figure 9	Stiffened Composite Patched Plate.....	19
Figure 10	Cross-sectional View of Stiffened Plate	20
Figure 11	Cross-sectional View of Smeared Plate.....	20
Figure 12	Smeared Composite Patched Plate.....	21
Figure 13	Single Side Strap Joint.....	21
Figure 14	Stress Distribution across Plate Thickness	21
Figure 15	Free Body Diagram.....	22
Figure 16	Four Plate Configurations Used.....	25
Figure 17	Maximum SERR for Varying Crack Length	26
Figure 18	Normalized SERR for Different Stiffener Configurations	27
Figure 19	SERR Distribution across the Thickness of the Plate.....	28
Figure 20	SERR for Varying Crack Location	29
Figure 21	Normalized SERR for Varying Crack location	29
Figure 22	SERR for Various Stiffener Separation	30
Figure 23	Normalized SERR for Various Stiffener Separation	31
Figure 24	Change in Stiffener Height	32
Figure 25	SERR for Varying Patch Stiffness.....	33
Figure 26	Flat Composite Plate Under Tensile Load	34
Figure 27	Comparison of Stress and SERR for Varying Patch Thickness	35
Figure 28	Flat plate with Center Crack	35
Figure 29	Cross Section Cut of Cracked Plate	36
Figure 30	Crack Displacement from a Tensile Load	36
Figure 31	Effect of an Infinitely Small Patch.....	36
Figure 32	Effect of Increasing Patch Stiffness.....	37
Figure 33	Normalized SERR vs. Stress.....	38
Figure 34	Maximum SERR for Varying Stiffener Height	39
Figure 35	SERR Distribution	40
Figure 36	Neutral Axis Location for Bending Moment.....	40
Figure 37	Various Plate Thicknesses while Applying a Bending Moment	41
Figure 38	Location of Maximum SERR	42

THIS PAGE INTENTIONALLY LEFT BLANK

LIST OF ACRONYMS AND ABBREVIATIONS

APDL	ANSYS Parametric Design Language
DOF	degree of freedom
FEA	finite element analysis
RAN	Royal Australian Navy
SCC	Stress Corrosion Cracking
SIF	Stress Intensity Factor
SERR	Strain Energy Release Rate
VCCT	Virtual Crack Closure Technique

THIS PAGE INTENTIONALLY LEFT BLANK

ACKNOWLEDGMENTS

I would like to thank Dr. Kwon, my thesis advisor, for his continued patience and guidance throughout the entire thesis process. I would also like to thank Dr. Lee for the numerous hours he spent instructing and assisting me to troubleshoot the finite element software.

THIS PAGE INTENTIONALLY LEFT BLANK

I. INTRODUCTION

A. BACKGROUND

The advancement of composite materials has led to an increase in its use for a wide variety of applications. Both the marine and aero industries have gravitated towards its use for its favorable properties. One application that has gained favorable attention in recent years is the use of composites for patches in the repair of cracks in aluminum structures.

During the service life of a vessel or aircraft, various repetitive loadings occur that in some cases have led to fatigue cracking. Fatigue cracks can continue to grow and adversely affect the structural integrity of the ship or aircraft. This scenario has plagued several recent classes of warships and aircraft [1], [2].

1. FFG-7

The Oliver Hazard Perry-class Frigates experienced severe fatigue cracking early in their service life. The ships were designed with a steel hull and a continuous aluminum superstructure welded to the deck. The shape of the superstructure created numerous stress concentration areas. Of the greatest concern was in the amidships area on the 02 level, where the structure necked down [1]. This led the U.S. Navy to implement several design modifications. The 02 level was strengthened by increasing the plate thickness in the region of the high stress concentration. The plates were also tapered to avoid creating additional stress concentrations [1].

The Royal Australian Navy (RAN) purchased six frigates with this design flaw from the United States [1]. For the RAN to implement the changes the U.S. Navy had made to solve the problem would have been costly and taken several maintenance availabilities that would have reduced the operational capability for its navy. The RAN looked for alternatives, which led it to composite patching. This method was applied to the HMAS Sydney (FFG 03) in 1998 and has been proven effective over the life of the ship [1]. As long as the composite did not debond from the deck, the crack growth did not

continue. If debonding did occur, the patch could be removed and reapplied without a substantial maintenance period [1].

2. CG-47

Similar to the Oliver Hazard Perry-class, the Ticonderoga-class Cruisers have a steel hull and aluminum superstructure. The superstructure for this class has also experienced severe crack growth [3]. However, in the case of the Ticonderoga, the cracking has been exhibited in areas of relatively low stress levels and is contributed to Stress Corrosion Cracking (SCC) [3]. For SCC to occur the following three factors must be met:

- The crack must occur on a sensitized material
- Tensile stresses must be present
- A corrosive environment must be present.

Composite patching aims to decrease the tensile stresses and thus stop the SCC. To date, three cruisers are using composite patching to reduce the growth of some instances of SCC [4].

3. Aeronautical Industry

The aircraft industry has been using composite materials for several decades with great success. The high strength-to-weight and stiffness-to-weight ratio of composites has naturally lent themselves to this field. This wide acceptance of composites has included their use as a method of repairing cracked aluminum surfaces [2]. Traditional methods of repair normally consisted of riveting an additional reinforcement onto the damaged area. This would create new defects and stress concentrations which could lead to additional cracking. On the other hand composite patches did not cause any further damage to the affected area and could be removed and reapplied several times if necessary. They were also found to be an easier method for quick repairs and could be formed around complex areas of an aircraft structure [2], [5].

B. LITERATURE REVIEW

Composite patching of cracks in aluminum structures has been studied to a great extent. There have also been several studies involving the effect that stiffening members have on crack growth. The following summary highlights the findings in these fields as it relates to this study.

1. Symmetric vs. Asymmetric Patching

Double-sided or symmetric patching is the strongest configuration when applying a composite patch. This has been shown as an effective means of lowering the Stress Intensity Factor (SIF) and in turn increasing the fatigue life [6], [7], [8]. Symmetric patching has been shown to provide a more even distribution of stress across the thickness of the plate. For the same configuration, Klung et al. have shown that a double-sided patch has twice the fatigue life of a single-sided patch [9].

Aircraft and ship structures are often inaccessible on one side and therefore do not lend themselves to symmetric patching. Or in some cases an aircraft would prefer to have a patch on the internal side of its skin to reduce drag. For these reasons, asymmetric patching is the most common application and has led to several studies (e.g., [3], [5], [10], [11]) to focus on this configuration. Asymmetric patching causes a shift in the neutral axis away from the center of the plate towards the patched side. The shift in the neutral axis introduces a bending moment that increases the stress on the unpatched surface and increases the force that the plate experiences [5]. This causes an increase in the SIF which in turn lowers the effectiveness of the patch [5].

2. Plate Thickness

The majority of studies on composite patching have modeled thin aluminum plates to represent the skin of an aircraft where patches have been predominantly used. The increasing use of composite patching for naval applications has led some studies (e.g., [3], [11]) to consider the significance of patching thicker plates. In order to conduct finite element analysis of a thick plate it is necessary to use a three-dimensional model [8]. Tsai et al. have conducted experimental and finite element comparisons of a thick

aluminum plate with various composite patch repairs [8]. They concluded that the location of the maximum Stress Intensity Factor (SIF) across the thickness of the plate varied with the patch configuration. It was located in the middle for the unpatched and double-sided case and on the free surface for the single-sided patch [8].

3. Patch Design

The design of the patch is composed of many different characteristics. Dimensions, orientation, shape and material properties have all been studied to find an optimal composite patch configuration.

For dimensions, patch thickness has been found to be the most crucial design criterion that determines the effectiveness of a patch. Kumar et al. have concluded that for a double-sided patch, increasing patch thickness is more important than increasing the surface area of a patch [7]. Patch thickness is still a vital component to consider when applying a single-sided patch. If the patch is too thick, then a large out-of-plane bending moment will be created, which will cause the patch to become detrimental and increase SIF [10].

Patch sequencing has been investigated extensively by Chue et al. who have found that orientation other than perpendicular to the crack has little benefit [12]. Applying a few plies in the 45-degree orientation would be effective in preventing cracks when biaxial and shear loads are applied. However, any plies in the direction parallel to the crack had little effect [12].

For shape, it has been shown that tapering the edge of the patch is vital to reducing the stress in the adhesive layer that would cause early failure of the patch [6].

Material properties of concern are the patch's modulus of elasticity and its thermal expansion coefficient. For asymmetric patching the modulus of elasticity has an influence of the neutral axis. The thermal expansion coefficient is important because the patch undergoes an exothermic reaction as it cures. This creates a residual stress that is discussed further in the next section [13].

4. Residual Stress

There are two main sources for residual stress in a stiffened plate with a composite patch. The first is caused from the exothermal reaction during the curing of the adhesive and patch. The aluminum plate has a much larger coefficient of thermal expansion than the composite patch. During the cooling process the plate wants to contract more than the patch which will create a tensile stress on the adhesive side and a compressive stress on the free surface. This gradient will create an out of plane bending moment that will have a tendency to close the crack on the free surface and in turn lower the crack growth [11]. To predict the level of residual stress created during this process the temperature that the adhesive affectively bonds to the aluminum plate is required [12]. This is rather difficult to predict so instead it is neglected in this study as it will help provide a conservative estimate.

In marine applications almost all stiffening members are attached by welding. Unlike a stiffener that has been riveted, a welded stiffener can allow a crack to propagate through, causing failure in both the plate and the stiffener [13]. The process of welding also creates a residual stress with a typical distribution, depicted in Figure 1.

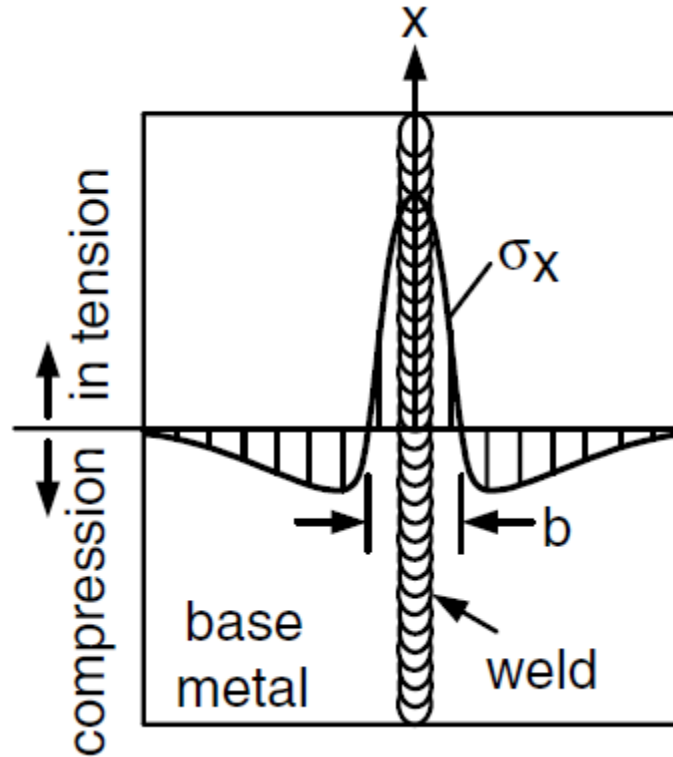


Figure 1 Typical Longitudinal Stress Distribution, from [16]

While the compressive stress will slow the crack growth if it continues toward the weld, it will experience a tensile stress that will cause the crack growth to accelerate. The residual effect of welded stiffeners on crack growth has been studied by Dexter et al. and modeled analytically. They also concluded that the principle of superposition can be applied to the stress intensity factor near a crack tip as long as it demonstrates linear elastic behavior [15], [17]. In the case of crack growth on a ship, the stress levels are often below the yield strength of the material so this assumption can be applied [15]. Since the magnitude and location of the residual stress caused by welding varies greatly with numerous parameters it is not considered in this study. Instead, it is noted that as the crack tip approaches the stiffening member the analytical model that Dexter et al. developed can be applied with the principle of superposition.

5. Stiffening Members

Poe conducted research on the effect that evenly spaced stringers, riveted to thin aluminum sheets, had on the SIF [17]. He found that for large cracks the SIF for a stiffened plate was much less than that of an unstiffened plate [17], while for small cracks the stiffeners had less of an effect on the SIF. He also concluded that, as the separation between the stiffening members decreased, so did the SIF [17].

Sabelkin et al. conducted both experimental and finite element research on composite patched plates with riveted stiffeners. The sheets were made of thin aluminum with an asymmetric patch on the same side as the stiffeners [18]. His research concluded that both a composite patch and stiffening members will decrease the SIF. Increasing the separation of the stiffeners decreases their effect and reduces the number of cycles until failure. A composite patch applied to an unstiffened plate will increase the fatigue life of the plate by tenfold; however, when applied to a stiffened plate the fatigue life will only increase by fivefold [18].

6. Analytical Models

Developing an analytical model for a patched plate allows for easy selection of patch parameters to reduce crack growth. Several analytical models have been developed for patched plates along with crack stiffened plates [4], [13]. There has yet to be one developed for a stiffened plate with a composite patch.

A key attribute to an analytical model is its ease of use. Kwon et al. developed an analytical model for a patched plate that creates a linear relationship between the normalized SERR obtained from FEA and stress in the base plate calculated analytically. An objective of this study is to find an approach to adapt a stiffened plate to the model created by Kwon et al. [17].

C. OBJECTIVES

There has been significant effort in the study of composites patching for thin flat aluminum plates. However, there has been much less focus on thicker plates or plates with stiffening members. These topics will be the primary focus of this study with the following objectives.

1. Develop a finite element model of a composite patched plate with stiffening members. The model must have the ability to adjust its parameters and be able calculate the SERR at the crack tips.
2. Develop an analytical model that can predict the decrease in the SERR for a stiffened plate after a composite patch has been applied.
3. Use the finite element model to investigate different stiffener parameters and determine the effect they have on the SERR.
4. Investigate the effect that plate thickness has on a patched and stiffened model.

II. FINITE ELEMENT MODEL

The finite model used in this study was intended to represent a portion of a ship's structure. To accomplish this, several features included in the model varied as they would throughout a ship's structure.

A. MODEL DESCRIPTION

The finite element model for this project was constructed with the geometry shown in Figure 2.

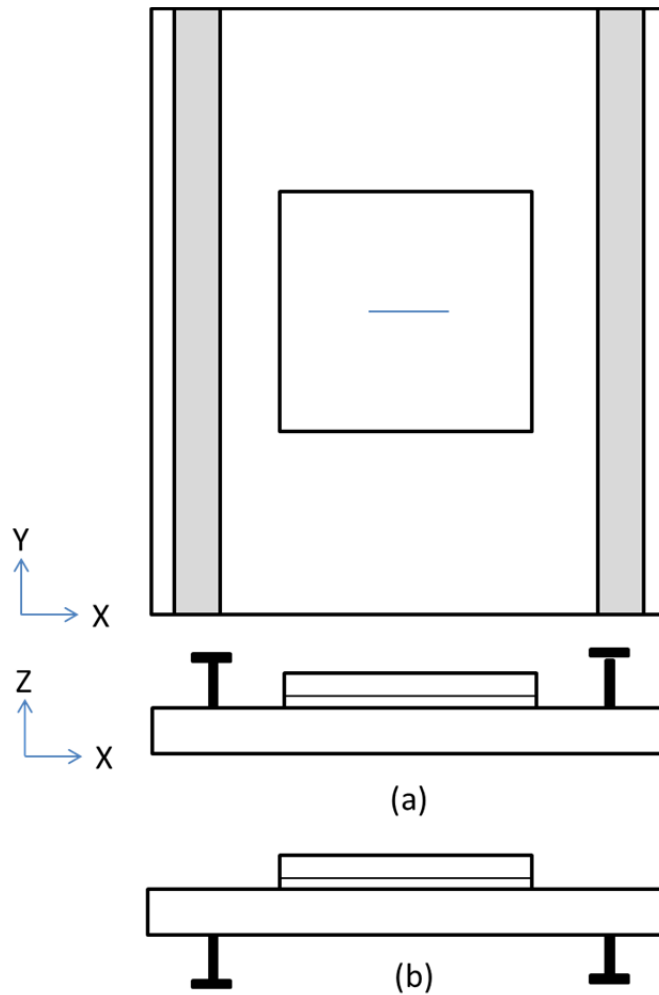


Figure 2 Model Geometry

The base of the model was a flat plate 0.61 meters (24 inches) long, 0.61 meters wide and 6.35 millimeters (0.25 inches) thick. A horizontal crack was modeled through the thickness of the plate. Both the crack's size and position varied along the x-axis. The material properties for the plate were selected to resemble aluminum, which is often susceptible to cracking.

A T-beam stiffener was used throughout this study. This was to represent one of the more common support members found in a ship's structure. The stiffeners in the model run the length of the plate, and they are depicted as grey rectangles in Figure 2. The stiffeners had two configurations; they were either on the same side or opposing side as the patch. The initial dimensions used for analysis can be seen in Figure 3.

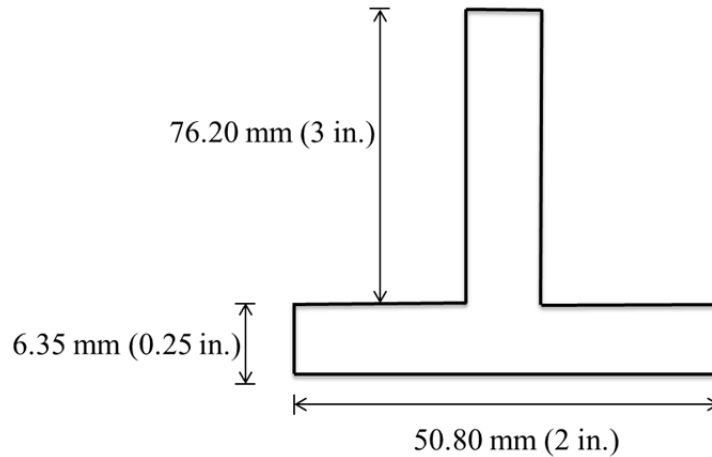


Figure 3 Stiffening Member Dimensions

Choosing and applying the correct boundary and load conditions to a finite element was a vital component in obtaining accurate results. Both a tensile load and bending moment were applied to the model to represent the forces experienced by a ship. Both of these loads were represented by applying a pressure to the ends and top of the plate, respectively. For both load conditions, the plate was modeled as a simply supported beam as illustrated in Figure 4.

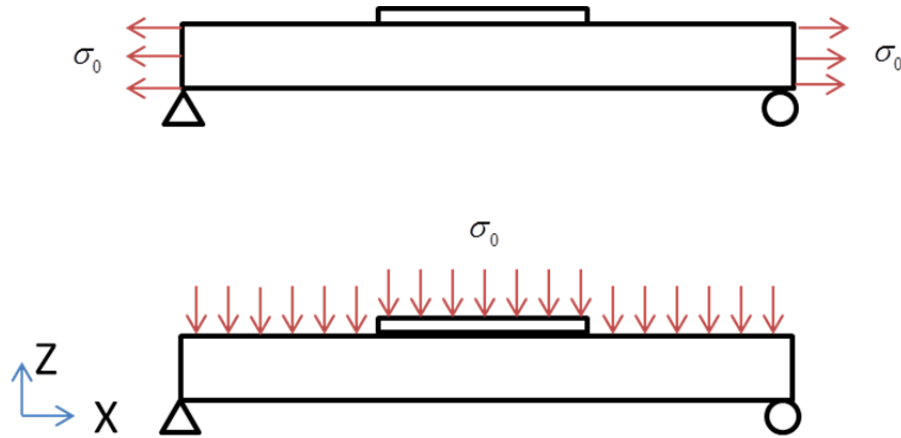


Figure 4 Boundary and Load Conditions

B. MODEL CONSTRUCTION

For analysis the model was constructed as a three-dimensional finite element using the commercially available software ANSYS. This model was constructed using a series of nested macros. ANSYS Parametric Design Language (APDL) is a scripting language that allowed the model to be built in terms of user defined parameters. This then made it possible to run a series of iterations that changes the model parameters and collected the necessary nodal data to calculate the SERR. Below is an overview of the functionality of each macro file.

- **Main:** The main program is the first file in the model creation preprocessor. This is where the design parameters are controlled and subroutine programs are called in sequence.
- **Set Up:** Creates empty arrays that are filled as the corresponding data is gathered. The size of these arrays varied depending on the number of iterations established in the main program file.
- **Delete Entries:** Prior to modeling the geometry, all stored parameters were cleared. This assures the data obtained for a run corresponds to the current models parameters.
- **Modeling:** The model geometry is created and meshed. There are several different modeling files that can be called. For each stiffener configuration there is a separate modeling file.

- **Set Boundary Conditions:** Selects the nodes and restricts their displacements. This file is the first file that starts the solution processor.
- **Apply Load:** For a tensile load the areas on each side of the plate are selected and a pressure load is applied of a magnitude that is designated in the main file. For the bending moment all areas on the top of the plate are selected and a corresponding pressure is applied.
- **Get Element and Nodal Numbers:** Extracts and assigns variables to the relevant element and node numbers that will be used in calculations.
- **Get Forces:** Extracts the relevant nodal forces near the crack tip and assigns a variable to be used in calculations.
- **Get Displacements:** Calculates the displacements in the x, y, and z direction for node pairs along the crack opening.
- **SERR:** This file calculates the SERR from the displacement and force values gathered in previous macro files. It then creates and writes them to text file where they are stored.

1. Element Selection

The plate, adhesive, and patch were all molded using a twenty-node solid brick element (SOLID186). The stiffening members instead used an eight-node shell element (SHELL281). The difficulty in using both shell and solid elements comes into play when attaching the two different element types. Where the two elements come into contact, the degrees of freedom (DOF) must match. A shell element has six DOF per node, which consist of three translational and three rotational. On the other hand, a solid element only has three translational DOF per node. To align the DOFs, an additional shell element was added as depicted in red in the Figure 5. The dimensions of these elements were decreased to the approximate size of a weld fillet but were still included in the analytical calculations.

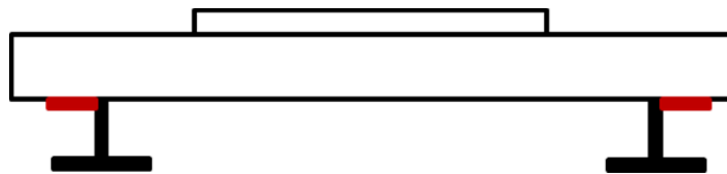


Figure 5 Alignment of Degrees of Freedom

Due to the varying parameters in this model it was not possible to take advantage of any symmetry. Instead, to decrease the computational time, the mesh size was varied. In the vicinity of the crack tip, very refined mesh was used; the farther from the crack, the courser the mesh became.

2. Linear vs. Nonlinear

There are three types of nonlinearities that are encountered in FEA. The first type is geometrical nonlinearities, which are caused from large displacements in the model. Material nonlinearities, the second type, are present when the material does not behave in a linear fashion. The third and most common type is boundary nonlinearities, when boundary conditions are dependent on displacement. The conditions necessary for geometric and material nonlinearities were not present in this study; however, boundary nonlinearities were a concern.

Contact problems are the most frequent occurrence of boundary nonlinearities. When two surfaces modeled in finite element analysis (FEA) come into contact with one another, penetration of one element's surface through an opposing element can occur if they are not properly defined. This is not an accurate physical representation of the model as it will not transmit normal and tangential friction forces and will lead to inaccurate results [19]. This issue can be resolved by defining the two surfaces as a contact and target surface, respectively, which is also known as a contact element pair. By doing this, the surfaces will not penetrate one another and transmit the correct forces.

Contact element pairs create a nonlinear solution and significantly increase the run time of the model. For this reason, they are only used when necessary. Contact of elements is more common in models with large displacements or rotations. While neither of these conditions exists in this model, previous studies that have applied a large bending moment to composite patched plates have experienced contact between the crack surfaces [3]. This is of concern for both loading conditions as the stiffening members and patch create a shift in the neutral axis when a tensile load is applied. This in turn creates a bending moment.

While visual inspection of the model revealed penetration only when a bending moment was applied, the contact element pair was still applied to the model for comparison. The top of the crack surface was modeled CONTA174 while the bottom was modeled with TARG170. For the tensile load, the model was run through a series of iterations with different stiffener heights so that the plate would experience various bending moments. Each of these iterations was run with and without the contact model applied. This revealed no difference in the results, and it was concluded that there was only contact when a bending moment was applied. Therefore, the contact element pair was only applied to the model when a bending moment was applied.

C. APPLICABLE THEORIES

For a crack to grow, the stress at the tip must exceed the cohesive strength of the material. Due to the sharp geometry of a crack tip, the stress concentration approaches infinity and is impossible to calculate [20]. This has led to the development of other criteria to model and predict crack growth.

1. Crack Growth Modeling

Stress Intensity Factor (SIF), K , is one of the most commonly used criteria in fracture mechanics. It characterizes the stress level in the plastic region of a crack tip. One of the important parameters that can be compared to the SIF is the rate of crack growth per cyclic load (da/dN). This relationship is established from the Paris' Law as seen in Equation (1), where C and m are material constants and ΔK is the SIF range.

$$\frac{da}{dN} = C \Delta K^m \quad (1)$$

Strain Energy Release Rate (SERR), G , is the other common criterion used to measure crack growth, especially when using FEA. SERR measures the change in potential energy per unit crack area surface. SERR and SIF are related by Equation 2.

$$G = \frac{K^2}{E} \quad (2)$$

Both SERR and SIF are normally expressed for a particular mode of fracture. There are three possible modes of fracture for a crack, as shown in Figure 6a through c.

Opening mode or mode I, as seen in Figure 6a, is the predominant one for this study. The shearing mode (mode II), as seen in Figure 6b, is the driving force for delamination of a composite patch. The tearing mode (mode III) (Figure 6c) is insignificant for this study and is only shown for reference. The modes for this study will be referenced by a roman numeral (i.e., G_I or K_I).

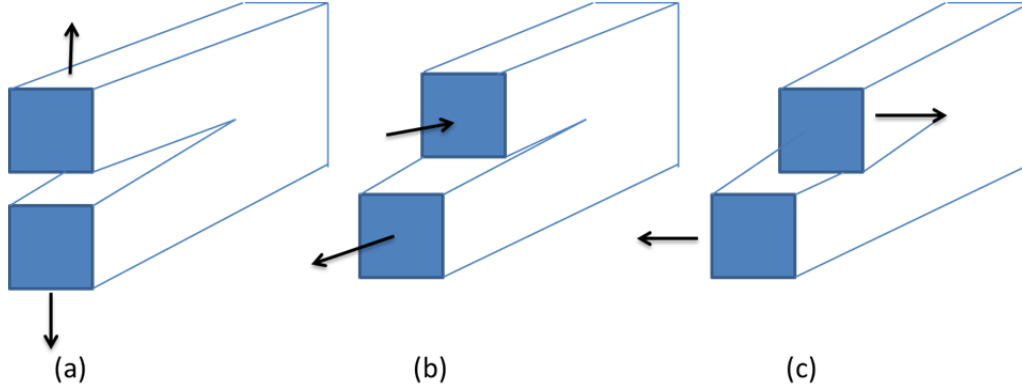


Figure 6 Three Modes of Fracture

2. Virtual Crack Closure Technique

To measure the SERR at the crack tip, the Virtual Crack Closure Technique (VCCT) was applied. This allowed for the extraction of both SERR mode I and II (G_I and G_{II}). To understand the VCCT it is helpful to examine it first in two-dimensions, as shown in Figure 7. The first step to applying this technique is modeling nodal points for the upper and lower surface of the crack with identical coordinates, while still allowing them to move independently. As a force is applied, the nodal points will separate; however, the crack will not be able to extend. VCCT makes several assumptions that account for this. First, the energy required to extend the crack a distance Δa is identical to the energy required to close the crack the same distance. Second, if the crack was able to extend, it would not significantly change the conditions at the crack tip. Meaning the energy required to extend the crack Δa is one-half the energy required to extend it a distance of $2\Delta a$ [21]. For the simple four-node two-dimensional example in Figure 7, the SERR would be:

$$G_I = \frac{\Delta Energy}{\Delta Area} = \frac{Force_y * Displacmen_y}{Area_{crack}} = \frac{-Z_i * \Delta w_{2l}}{2\Delta a} \quad (3)$$

$$G_{II} = \frac{\Delta Energy}{\Delta Area} = \frac{Force_x * Displacmen_x}{Area_{crack}} = \frac{-X_i * \Delta u_{2l}}{2\Delta a} \quad (4)$$

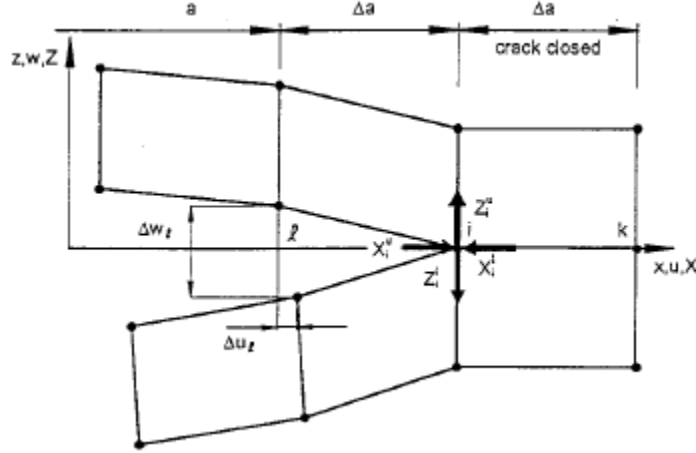


Figure 7 VCCT for Two-dimensional Element, from [6]

Applying this method to a three-dimensional 20-node element requires some additional considerations. The SERR is calculated for every nodal position at the crack tip across the thickness of the element. The nodal displacements and forces on both sides are also included for each calculation. For locations where a mid-side node is located, the calculations will have an additional force and displacement. Equations (5) and (6) were used to calculate G_I and G_{II} for corner nodes, whereas Equations (7) and (8) were used for mid-side nodes [21]. Figure 8 a and b depict the notation used in both the mid-side and corner node calculation, respectively.

$$G_I = -\frac{1}{2\Delta A_L} \left[\begin{aligned} &\frac{1}{2} Z_{Ki} (w_{Kl} - w_{Kl*}) + \frac{1}{2} Z_{Lj} (w_{Ll} - w_{Ll*}) \\ &+ Z_{Lj} (w_{Lm} - w_{Lm*}) + \frac{1}{2} Z_{Mi} (w_{Ml} - w_{Ml*}) \end{aligned} \right] \quad (5)$$

$$G_{II} = -\frac{1}{2\Delta A_L} \left[\begin{aligned} &\frac{1}{2} X_{Ki} (u_{Kl} - u_{Kl*}) + \frac{1}{2} X_{Lj} (u_{Ll} - u_{Ll*}) \\ &+ X_{Lj} (u_{Lm} - u_{Lm*}) + \frac{1}{2} X_{Mi} (u_{Ml} - u_{Ml*}) \end{aligned} \right] \quad (6)$$

$$G_I = \frac{1}{2\Delta A_M} \left[\begin{aligned} &\frac{1}{2} Z_{Li} (w_{Li} - w_{Li*}) + \frac{1}{2} Z_{Lj} (w_{Lm} - w_{Lm*}) + Z_{Mi} (w_{Ml} - w_{Ml*}) \\ &+ \frac{1}{2} Z_{Ni} (w_{Nl} - w_{Nl*}) + \frac{1}{2} Z_{Nj} (w_{Nm} - w_{Nm*}) \end{aligned} \right] \quad (7)$$

$$G_{II} = -\frac{1}{2\Delta A_M} \left[\begin{aligned} &\frac{1}{2} X_{Li} (u_{Li} - u_{Li*}) + \frac{1}{2} X_{Lj} (u_{Lm} - u_{Lm*}) + X_{Mi} (u_{Ml} - u_{Ml*}) \\ &+ \frac{1}{2} X_{Ni} (u_{Nl} - u_{Nl*}) + \frac{1}{2} X_{Nj} (u_{Nm} - u_{Nm*}) \end{aligned} \right] \quad (8)$$

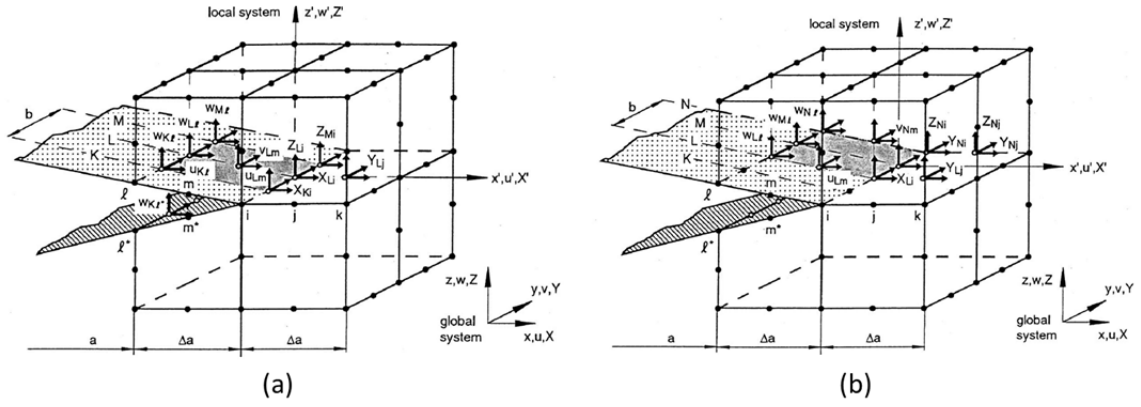


Figure 8 VCCT for Three-dimensional Elements, from [20]

THIS PAGE INTENTIONALLY LEFT BLANK

III. ANALYTICAL MODEL

The method of developing an analytical model for the stiffened patch plate closely resembled the process used by Kwon et al. [11]. First, a technique of relating the stiffened plate to an unstiffened plate was established. Next, the axial and bending stresses in the plate were solved for. These stresses were then normalized with respect to the maximum applied stress. Relations that compare the SERR to these normalized stresses were then applied. This in turn allowed for a linear relationship between the normalized SERR and normalized stress to be developed.

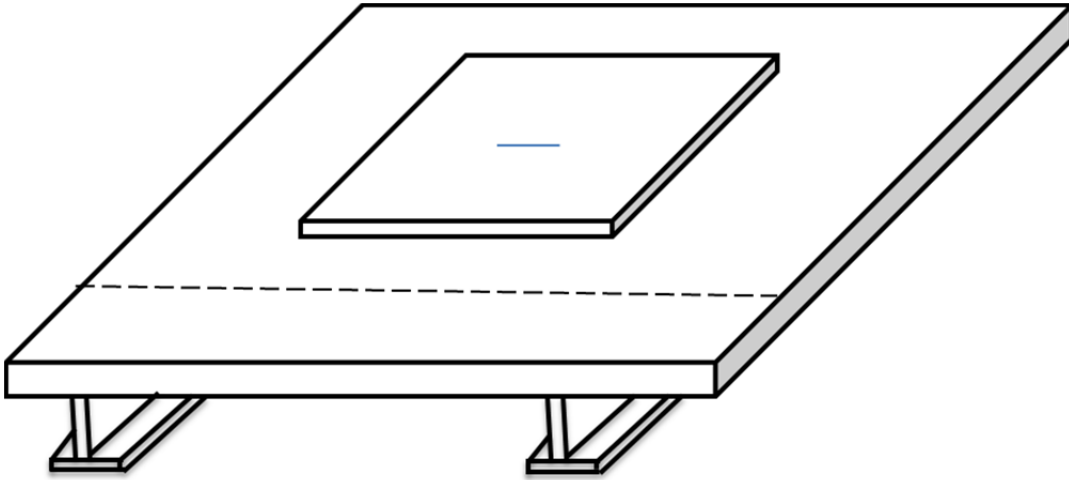


Figure 9 Stiffened Composite Patched Plate

The first step in solving the analytical model for the stress in the composite patched plate was finding a way to incorporate the stiffening members. A smearing technique was used to accomplish this. To illustrate this method, the cross-sectional cut of the stiffened plate depicted in Figure 9 was made along the dotted line. This resulted in the cross-sectional view of the stiffened plate, as seen in Figure 10.

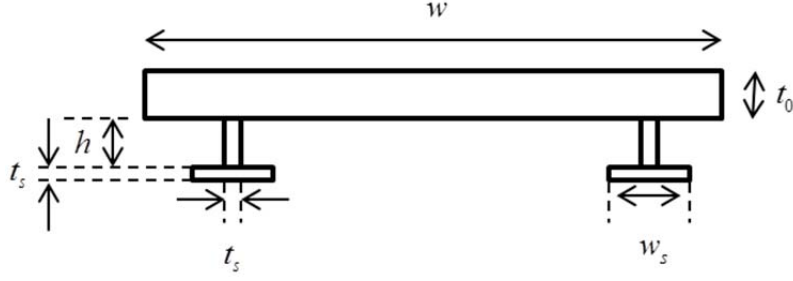


Figure 10 Cross-sectional View of Stiffened Plate

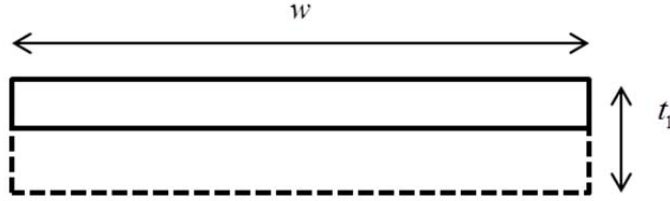


Figure 11 Cross-sectional View of Smeared Plate

The goal of the smearing technique was to find the equivalent thickness for the smeared model, depicted in Figure 11, so that it will react the same way as the stiffened model. To do this, the moment of inertia about the longitudinal direction was taken for both the stiffened model and the smeared model.

$$I_{stiffened} = \frac{1}{12} w t_0^3 + t_0 w \left(\frac{t_0}{2} - \bar{y} \right)^2 + 2 \left(\frac{1}{12} t_s h^3 + h t_s \left(t_0 + \frac{h}{2} - \bar{y} \right)^2 \right) + 2 \left(\frac{1}{12} w_s t_s^3 + w_s t_s \left(t_0 + h + \frac{t_s}{2} - \bar{y} \right)^2 \right) \quad (9)$$

$$I_{smeared} = \frac{1}{12} w t_1^3 \quad (10)$$

By setting both of these moments equal to one another, the plate thickness for the smeared model can be solved for.

$$I_{stiffened} = I_{smeared} \quad (11)$$

$$t_1 = \left(\frac{12 I_{stiffened}}{w} \right)^{\frac{1}{3}} \quad (12)$$

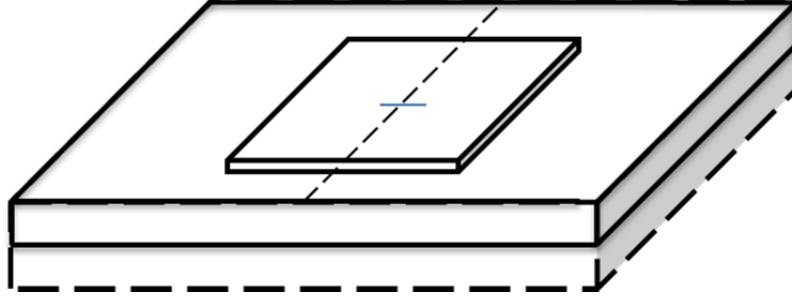


Figure 12 Smeared Composite Patched Plate

With the stiffeners excluded, the composite patch and smeared plate can be simplified as a single-sided strap joint. This is obtained by taking another cross-sectional cut perpendicular to the crack, as seen in Figure 12. Now, the stress distribution across the plate thickness can be solved for. This is accomplished by examining the midsection depicted by the dotted line in Figure 13.

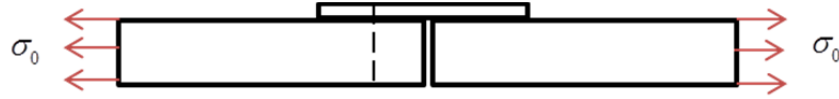


Figure 13 Single Side Strap Joint

A composite plate with a tensile load applied has two stress components, an axial and bending stress, as seen in Figure 14.



Figure 14 Stress Distribution across Plate Thickness

The average axial and bending stress can be approximated by the expressions in Equation (13) and (14), respectively [22].

$$\sigma_{axial} = \frac{1}{2} [\sigma_{max} + |\sigma_{min}|] \quad (13)$$

$$\sigma_{axial} = \frac{1}{2} [\sigma_{\max} - |\sigma_{\min}|] \quad (14)$$

To solve for both stress components, a free body diagram, as seen in Figure 15, was developed from a section cut made along the dotted line in Figure 13. The patch and plate have vastly different material properties, so the transformed section method was used to analyze this section. The adhesive layer is assumed to be small enough that its effect is negligible and is not included in these calculations.

The smearing technique significantly changes the distance from the bottom of the plate to the neutral axis. This increases the moment and maximum bending stress. The location of concern is still the bottom of the original plate represented by the thick dotted line in Figure 15.

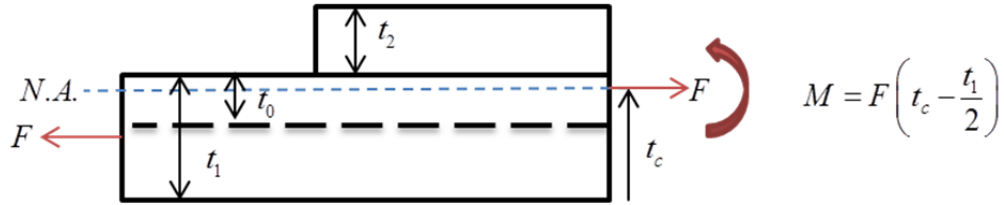


Figure 15 Free Body Diagram

This is the point at which the maximum bending stress is calculated for,

$$\sigma_{\min} = \frac{F}{A_{eq}} + \frac{M(t_c - t_1)}{I_{eq}} \quad (15)$$

$$\sigma_{\max} = \frac{F}{A_{eq}} + \frac{M(t_0 - (t_1 - t_c))}{I_{eq}}, \quad (16)$$

where A_{eq} and I_{eq} are the equivalent area and moment of inertia for the cross section. To simplify the calculations, a unit width was assumed.

$$I_{eq} = I_{plate} + nI_{patch} \quad (17)$$

$$A_{eq} = t_{plate} + nt_{patch} \quad (18)$$

The variable n is the modular ratio and is defined by the ratio of the modulus of elasticity of the two materials.

$$n = \frac{E_{patch}}{E_{plate}} \quad (19)$$

The neutral axis, defined by the variable t_c , is located where the bending stress equals zero. Using the bottom of the plate as a reference and by applying the equilibrium equations, the following expression is obtained.

$$t_c = \frac{E_1 t_1^2 + E_2 t_2 (2t_1 + t_2)}{2(E_1 t_1 + E_2 t_2)} \quad (20)$$

The force applied to the plate remained constant throughout this study and the thickness of the smeared plate varied depending on the characteristics of stiffening members. This resulted in a maximum stress for an unpatched case to also vary.

$$\sigma_0 = \frac{F}{t_1} \quad (21)$$

The normalized axial and bending stress was used for comparison.

$$\bar{\sigma}_{axial}^{norm} = \frac{\sigma_{axial}}{\sigma_0} \quad (22)$$

$$\bar{\sigma}_{bend}^{norm} = \frac{\sigma_{bend}}{\sigma_0} \quad (23)$$

For an unpatched plate, the SERR is proportional to the square of the applied stress.

$$G_{np} \propto (\sigma_0)^2 \quad (24)$$

The SERR for the patched plate is proportional to the square of the total SIF.

$$G_p \propto (K_{Total})^2 \quad (25)$$

For linear elastic materials, the stress intensity factors of the same mode of factor are additive [21].

$$K_{Total} = K_{axial} + K_{bend} \quad (26)$$

For the patched plate, the axial and bending stress affect the SERR. The relation that the axial stress has with a symmetric patch is still relevant for a single-sided patch [4],

$$K_{axial} \propto \frac{\sigma_{axial}}{1 + Sa} \quad (27)$$

where the axial stiffness ratio, SA, is defined as

$$SA = \frac{E_2 t_2}{E_1 t_1}. \quad (28)$$

Bending stress is only relevant to single sides patch and has been found to have the following relations to SIF [17].

$$K_{bending} = \frac{\sigma_{bend}}{\sqrt{2a}} \quad (29)$$

From the Equations (24) through (29) it can be concluded that

$$G_p \propto \left(\frac{\sigma_{axial}}{1 + SA} + \frac{\sigma_{bend}}{\sqrt{2a}} \right)^2. \quad (30)$$

To normalize the SERR for the patched plate Equation (30) is divided by Equation (24).

$$\frac{G_p}{G_{np}} \propto \left(\frac{\bar{\sigma}_{axial}}{1 + SA} + \frac{\bar{\sigma}_{bend}}{\sqrt{2a}} \right)^2 \quad (31)$$

IV. RESULTS AND DISCUSSION

The result and discussion section of this report is separated by the load condition applied to the model. The tensile load is the more predominate of the two and is covered first.

A. TENSILE LOAD

For the tensile load, several different parameters were investigated. They are presented in the order of their examination.

1. Change in Crack Length

The first parameter that was investigated was the length of the crack. A series of iterations were run that changed the crack length from 25.4 mm (1 in.) to 152.4 mm (6 in.). This was done for the following four configurations. Figure 16 describes these configurations with the corresponding color that is used in the graphs for this section of the report.



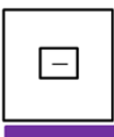
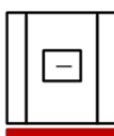
	Unstiffened and Unpatched
	Stiffened and Unpatched
	Unstiffened and Patched
	Stiffened and Patched

Figure 16 Four Plate Configurations Used

Figure 17 depicts the maximum SERR of the four configurations listed above for varying crack lengths. For the standard dimensions used in this study, both the patch and stiffener decrease the SERR. This corresponds with the experimental study that Sabelkin et al. conducted on thin aluminum plates [12]. Varying the stiffener height can change this result, and is discussed later in this report. As the crack length is increased, the effect that both the stiffening member and patch have increases. This is represented in Figure 18, which compares the ratio of the SERR for the patched and unpatched case. When this normalized value decreases, it means the patch has a greater effect on minimizing the SERR. From this comparison, it can also be seen that a patch decreases the SERR by a greater magnitude for a stiffened plate versus a non-stiffened plate. This result does not correspond with the previous study on thin plates [14]. This comparison was run both with the stiffener on the same side and on opposing sides. It was also shown that applying the patch on the opposite side of the stiffeners was the more effective configuration. For application on a ship, the opposing side is normally the more accessible side, and therefore is the configuration that is used for the remainder of this study.

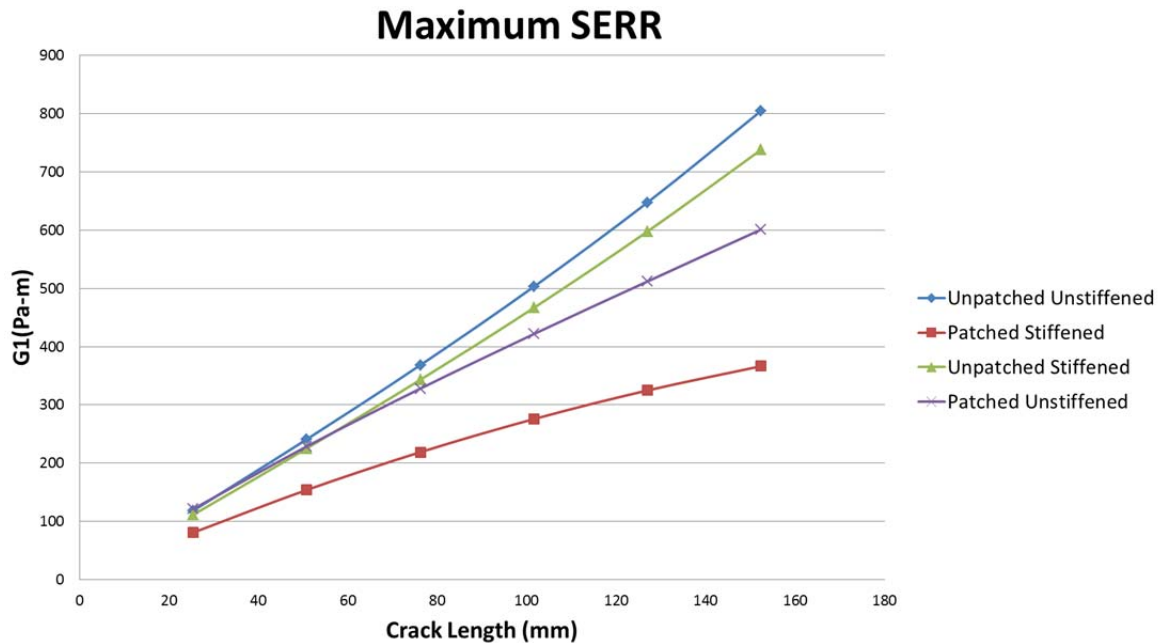


Figure 17 Maximum SERR for Varying Crack Length

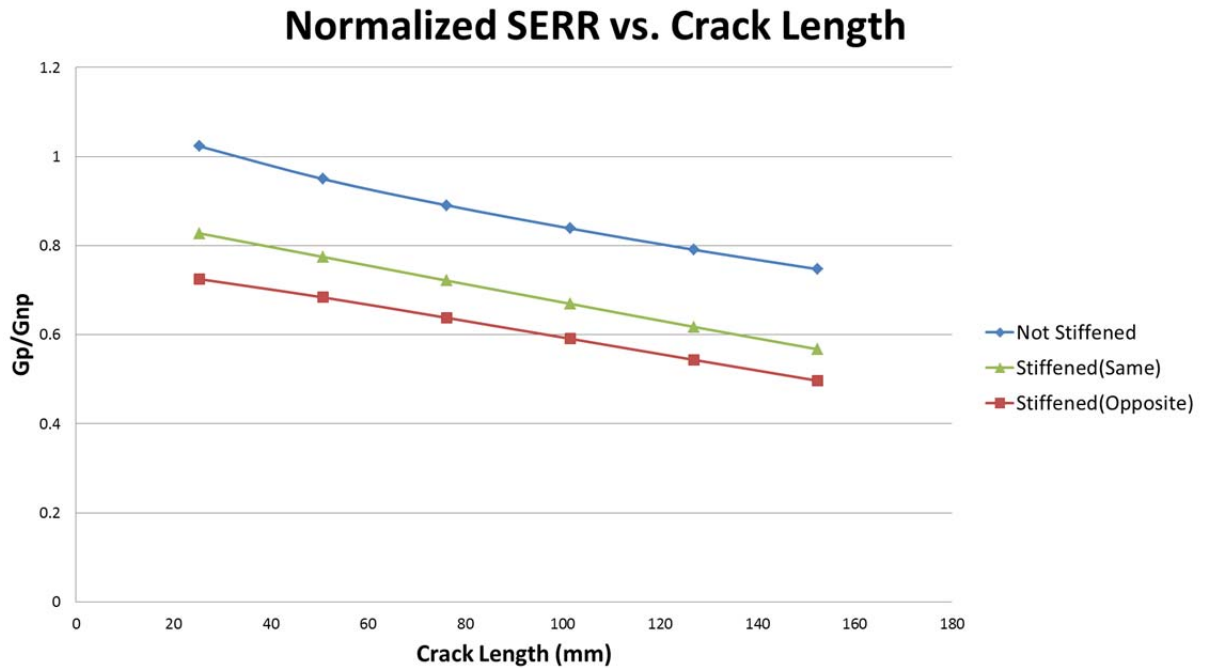


Figure 18 Normalized SERR for Different Stiffener Configurations

The location of the maximum SERR varied for different configurations. When the plate is unpatched and unstiffened, the maximum SERR is located in the middle of the plate. When a stiffening member is added, the SERR is decreased and the maximum SERR is shifted toward the unstiffened side. Whenever a patch is applied, the maximum SERR will be on the free side. This is shown in Figure 19 for the crack length of 50.8 mm (2 in.).

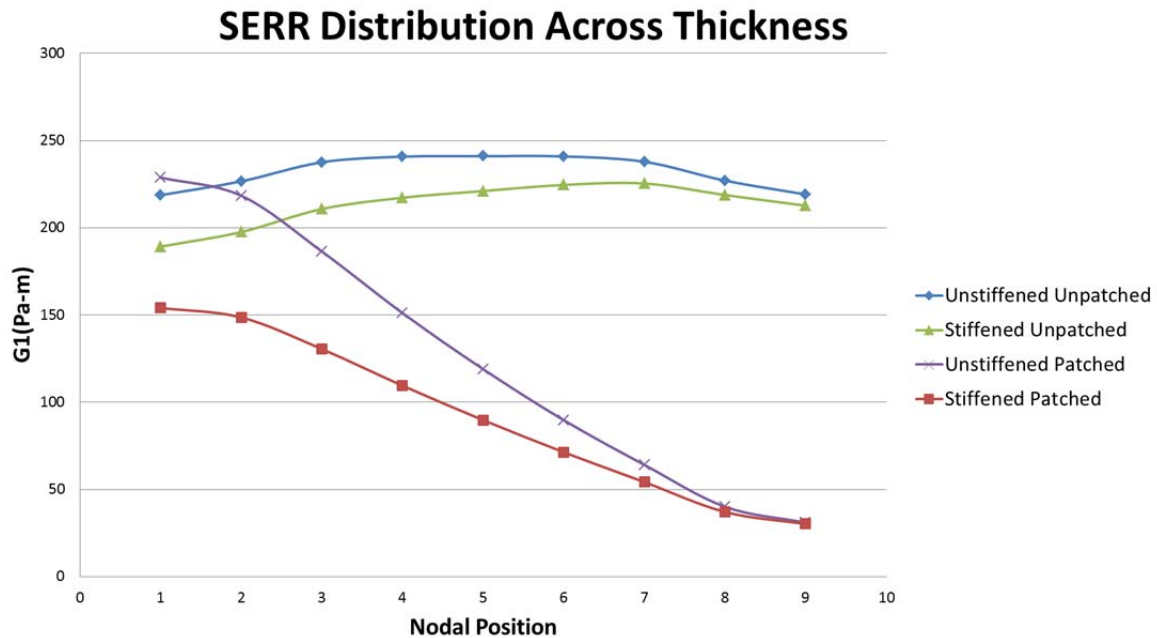


Figure 19 SERR Distribution across the Thickness of the Plate

2. Change in Crack Location

Crack location was the second parameter to be tested. A crack of 50.8 mm (2 in.) in the center of the plate was used. For each iteration that was run, the crack was moved 12.7 mm (0.5 in.) along the x-axis. The patch remained centered on the crack as this would be the logical method when applying a patch. The stiffening members were separated a distance of 558.8 mm (22 in.). All other parameters as described in Chapter II were kept constant.

As seen in Figure 20, the SERR for both crack tips decreases as it approaches the stiffening members. The crack tip closer to the stiffening member has a smaller SERR. In the absence of other influences this would cause the crack to grow away from the stiffening member more than toward it.

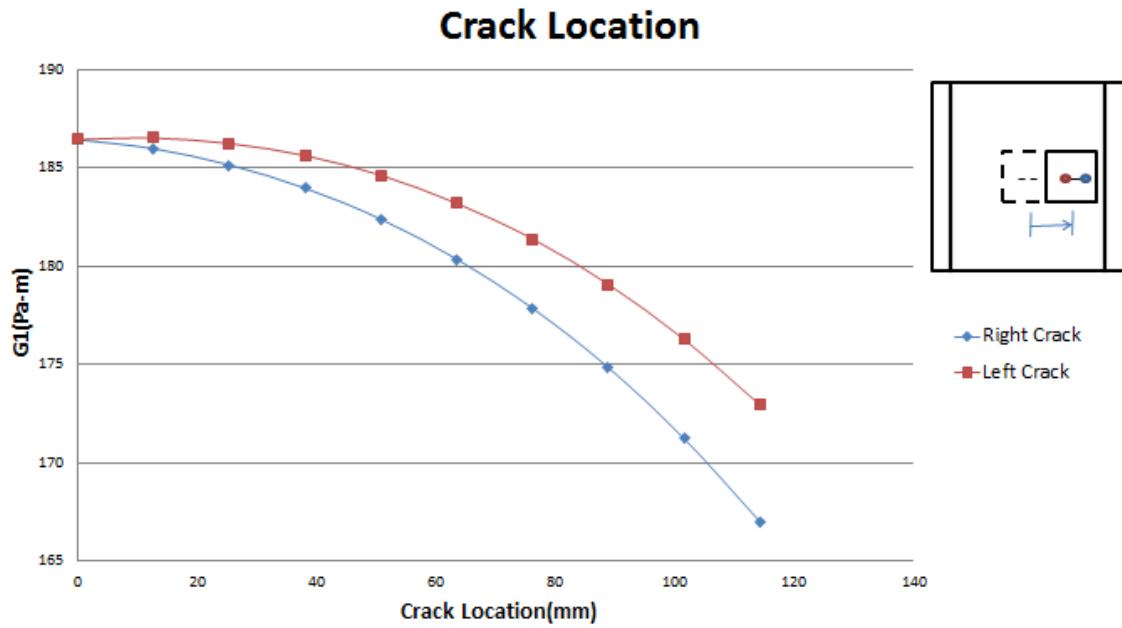


Figure 20 SERR for Varying Crack Location

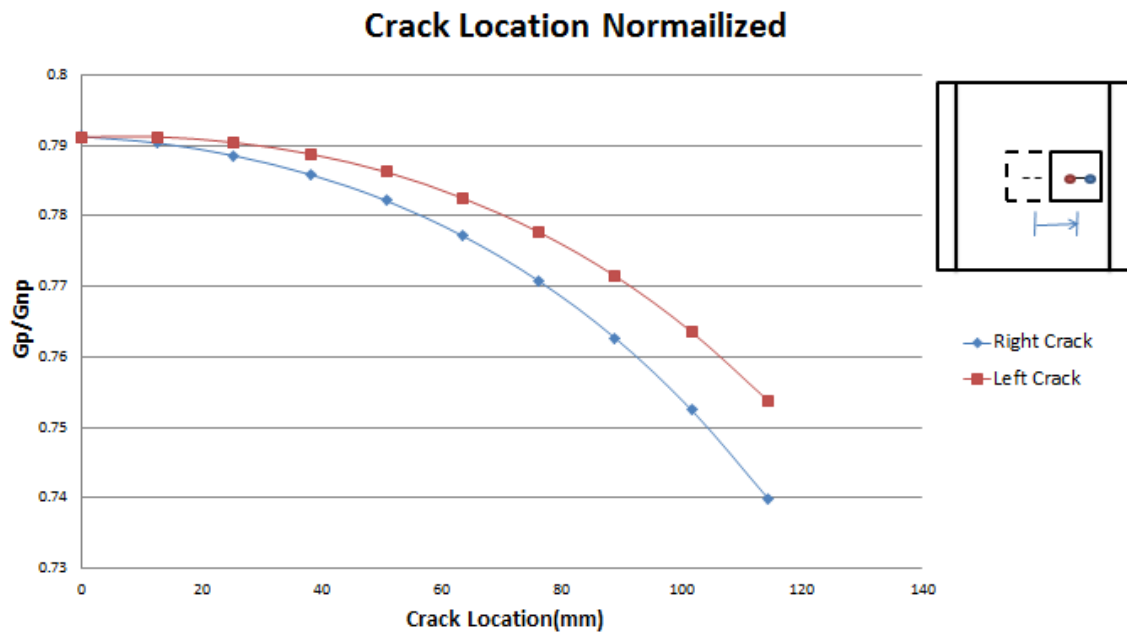


Figure 21 Normalized SERR for Varying Crack location

3. Change in Stiffener Parameters

Two parameters for the stiffening members were varied in this study. The height and span between stiffeners can characterize most of the differences found throughout a ship's structure.

As the distance between the stiffeners increases, the SERR also increases for both the patched and unpatched configuration. This can be seen in Figure 22. The increase in separation also decreases the effect of the patch. This can be seen with plot of the normalized SERR in Figure 23.

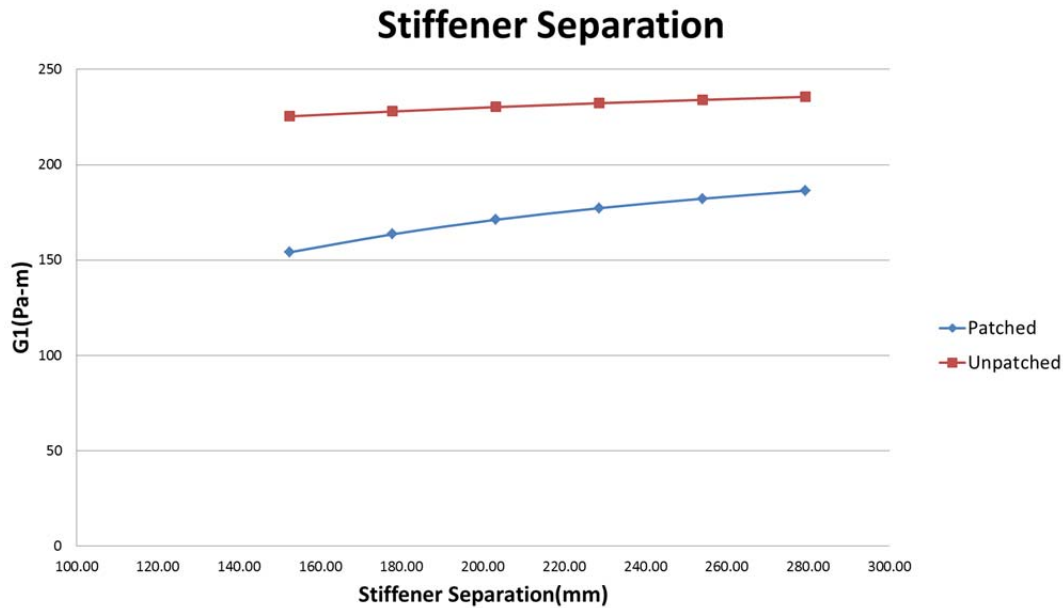


Figure 22 SERR for Various Stiffener Separation

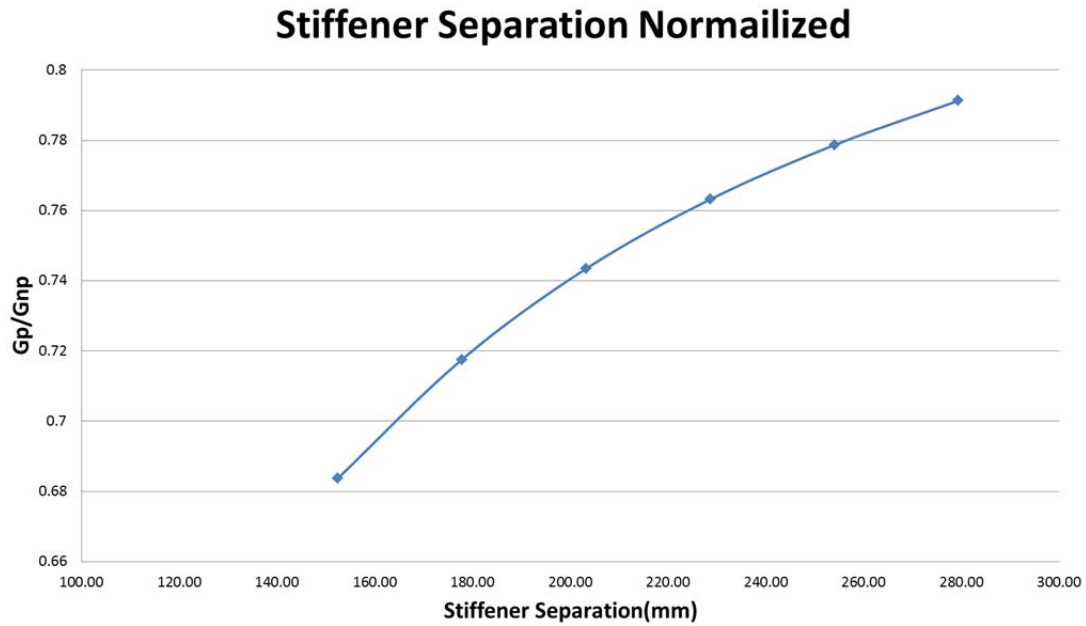


Figure 23 Normalized SERR for Various Stiffener Separation

The next stiffener parameter that was investigated was the height of the stiffener. The thickness and flange width remained constant but the distance from the flange to the base plate increased from 2.54 mm (0.1 in.) to 127.00 mm (5 in.) in increments of 2.54 mm (0.1 in.).

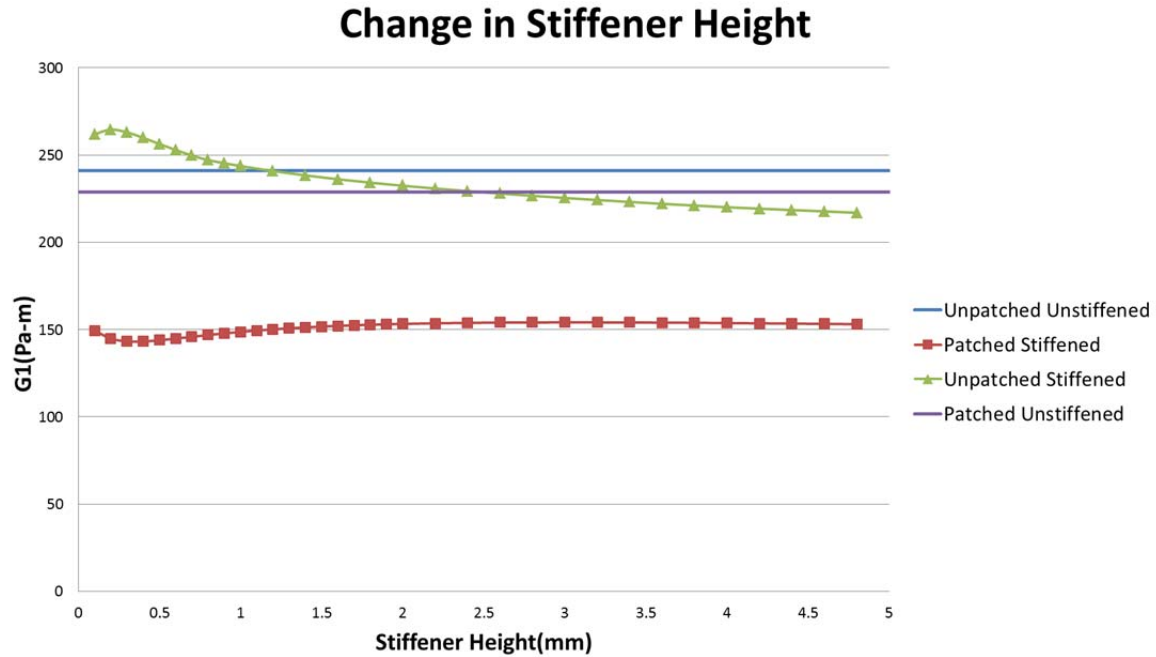


Figure 24 Change in Stiffener Height

As seen in Figure 24, stiffener height has an import impact on the SERR. An unpatched plate with a short stiffener has a higher SERR than an unstiffened plate. As the stiffener height was increased, the SERR decreased; eventually, the stiffened model became more effective than the unstiffened model at decreasing the SERR. Regardless of stiffener height, applying a patch was effective at lowering the SERR for a stiffened plate. Applying the stiffeners to a flat plate shifts the neutral axis, and was found to have an important effect on the SERR. To better understand this, other parameters that influence the neutral axis were investigated.

4. Change in Neutral Axis

The location of the neutral axis for a composite patched plate shifts when one or more of the material properties or dimensions are changed. To examine this more closely, a thick plate was examined without the stiffening members. Three parameters were examined for this scenario. First, the plate thickness changed while maintaining constant patch properties. Next, the plate thickness was fixed and the patch thickness varied. This was done several times while increasing the patch's modulus of elasticity.

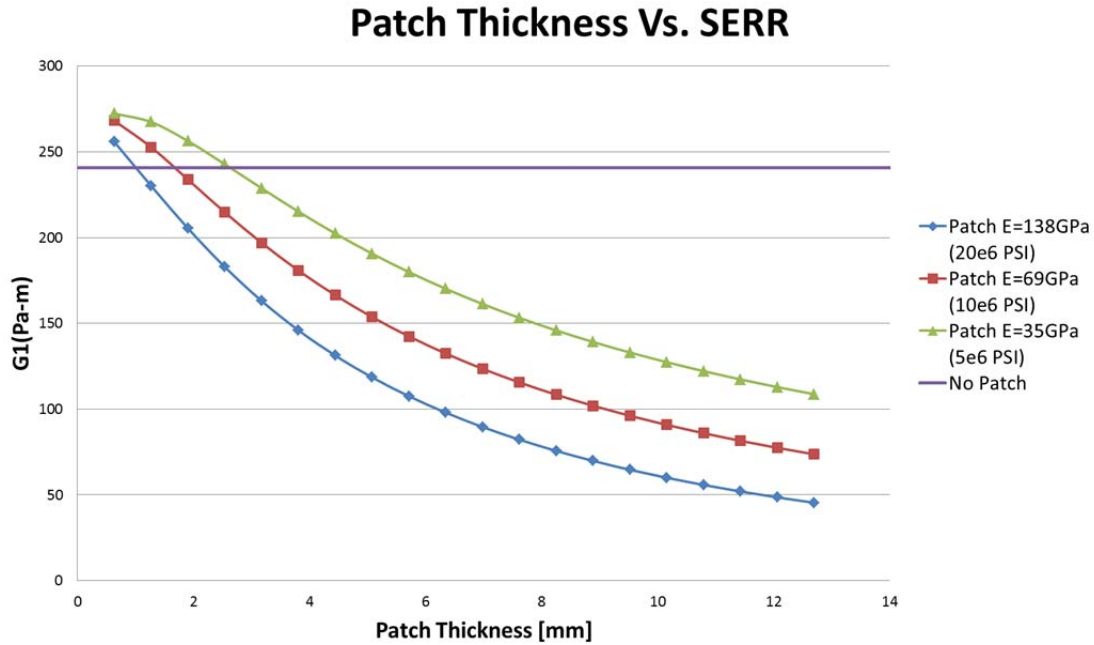


Figure 25 SERR for Varying Patch Stiffness

Figure 25 compares the SERR for a plate of constant thickness and a patch with varying properties. As the stiffness of the patch was decreased, the maximum SERR for the patched case is greater than that with no patch. This consistently occurred when the neutral axis was roughly below 63 percent of the plate's thickness. When the patch properties were held constant and the plate thickness varied, this relation still held true. This emphasizes the importance of selecting the correct patch properties. If a patch is applied with a low stiffness compared to the plate, it can have a detrimental effect and increase crack growth.

To better understand the importance the neutral axis location has on the SERR, the stresses involved for a composite plate were closely examined. A flat composite patched plate under a tensile load experiences an axial and bending stress. As the stiffness of the composite patch increases, the maximum axial stress will decrease. This relation can be seen in Figure 26, and is governed by Equations (32) through (34).

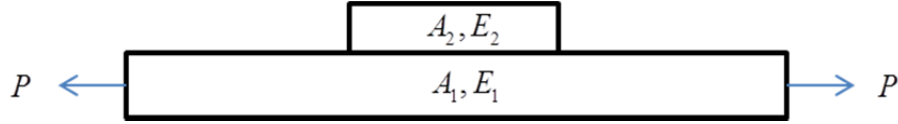


Figure 26 Flat Composite Plate Under Tensile Load

$$\sigma = \sigma_{axial} + \sigma_{bending} \quad (32)$$

The bending stress is created by a shift in the neutral axis. As the stiffness of the patch is increased, the bending stress will also increase.

$$\sigma_{axial} = \frac{P}{A_1 + A_2 \frac{E_2}{E_1}} \quad (33)$$

An increase in the bending stress and decrease in axial stress creates a local maximum. This maximum is dictated by the location of the neutral axis, and occurs when it is raised roughly 70 percent of the plate's thickness.

$$\sigma_{bending} = \frac{Mt_c}{I_{eq}} \quad (34)$$

While the total stress reaches a maximum, the SERR at the crack tip will continue to decrease as the patched stiffness is increased. The SERR will be greater for the patched case than that of the non-patched when the neutral axis is below 63 percent of the plate's thickness. All of these relations are represented for a case of varying patch thickness in Figure 27.

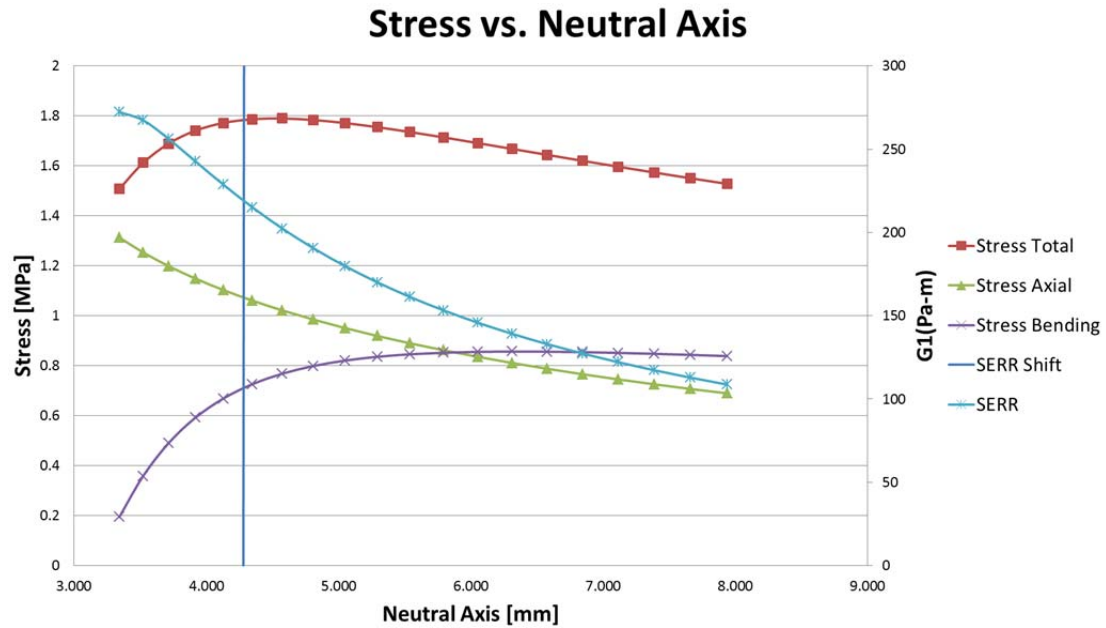


Figure 27 Comparison of Stress and SERR for Varying Patch Thickness

The reason for this occurrence can be better explained with a physical representation of how a patch influences a crack.

A flat plate with a centered crack, as seen in Figure 28, can be represented with the cross-sectional view in Figure 29.

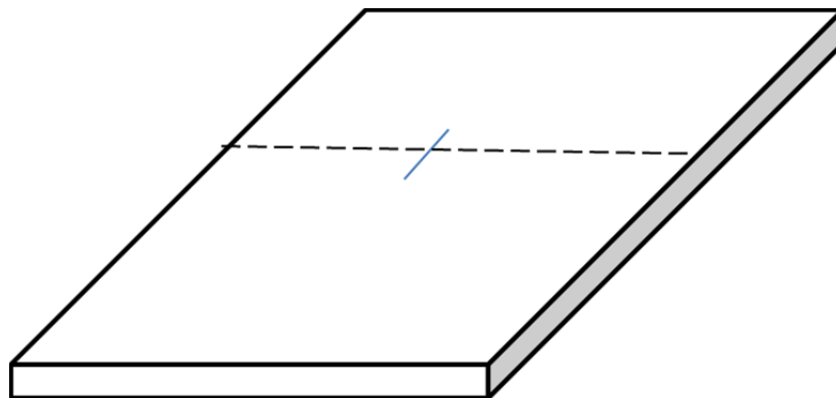


Figure 28 Flat plate with Center Crack



Figure 29 Cross Section Cut of Cracked Plate

When a tensile load is applied to the plate, the crack will open up a distance, δ_1 , evenly across the thickness, as portrayed in Figure 30.

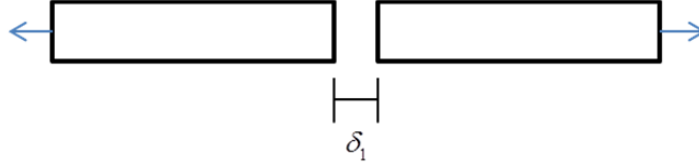


Figure 30 Crack Displacement from a Tensile Load

Suppose an infinitely small patch is applied to the plate. This would constrain the top of the plate but the bottom would be free to separate a distance δ_2 . If both cases represented in Figure 30 and Figure 31 were identical with the exception of the constraint, then δ_2 would be greater than δ_1 .

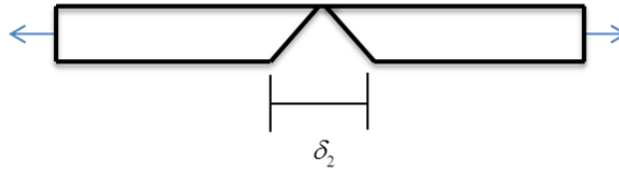


Figure 31 Effect of an Infinitely Small Patch

As the stiffness of the patch is increased, the bending stress is also increased while the axial stress is decreased. This will cause the opening at the bottom of the plate to close, which corresponds to the decrease in SERR (as seen in Figure 27). When stiffness of the patch raises the neutral axis to approximately 70 percent of the plate thickness, then the separation represented in Figure 32 will equal that in Figure 30. This corresponds to the point at which the SERR for the patched case is equal to that of the unpatched.

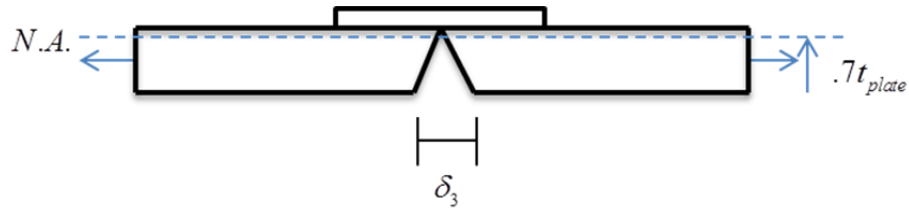


Figure 32 Effect of Increasing Patch Stiffness

The 7 percent difference is contributed to the SERR distribution for the unpatched case. The maximum occurs in the middle of the plate, which does not compare exactly to an even distribution, as depicted in Figure 30. When the SERR value is taken at the location that is used to calculate the stress, then the difference is decreased to less than 2 percent.

5. Analytical Comparison

Figure 33 compares the normalized SERR for all of the cases discussed previously with the normalized stress calculated using Equation (31). The linear relationship established validates the analytical expression developed in Chapter III.

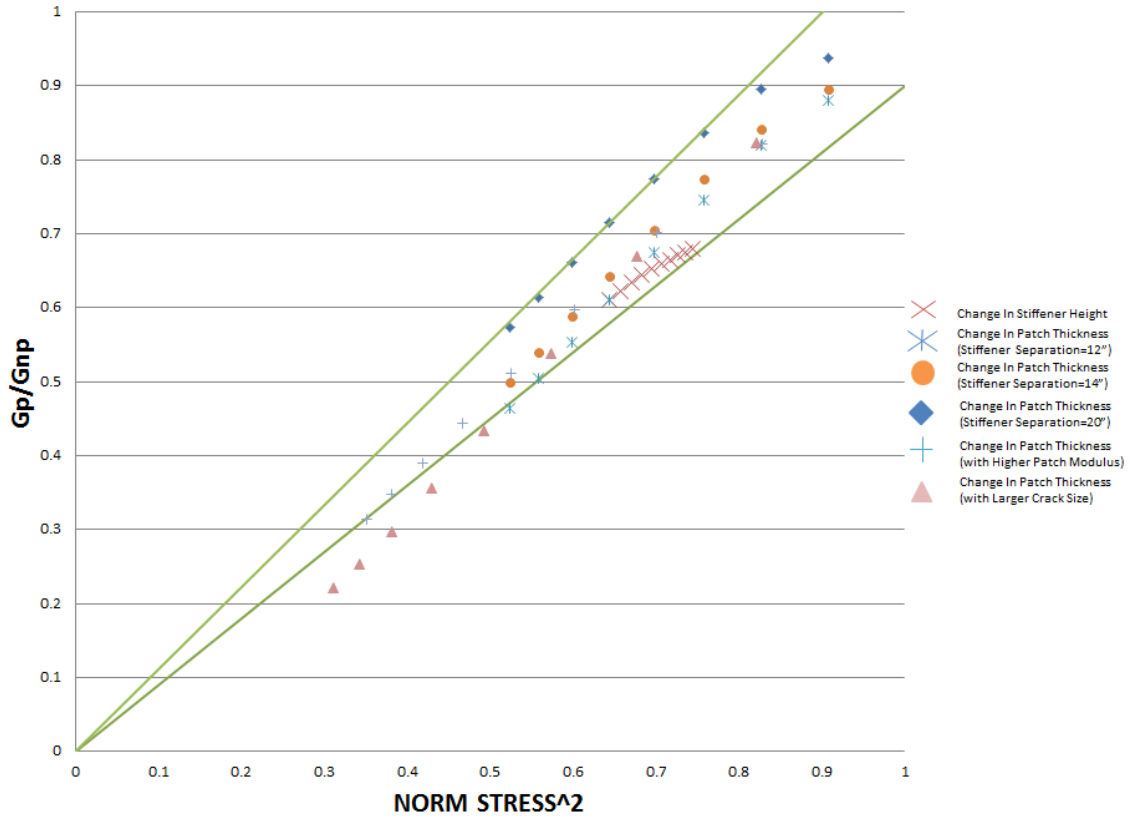


Figure 33 Normalized SERR vs. Stress

The smearing technique does not take into account the separation between the stiffening members. This causes the data to have some vertical separation. The closer the stiffeners are to one another, the more conservative this analytical expression becomes.

The usefulness of this expression comes from its ability to calculate the effectiveness of a patch when applied to a stiffened plate. Using the expression in Equation (31) and inputting the applicable parameters, the normalized stress is calculated. This can be compared with the linear relation to then solve for the normalized SERR. This value represents the reduction in SERR that obtained when the patch is applied.

B. BENDING MOMENT

When the bending moment was applied contact element pairs had to be used, which created a nonlinear solution. This significantly increased the run time of the model, and only two parameters were investigated. Both the stiffener height and plate thickness

had a significant effect for a tensile load, so they were also examined when a bending moment was applied.

1. Change in Stiffener Height

Stiffener height was the first parameter that was investigated when applying a bending movement. This was run from 2.54 mm (0.1 in) to 99.06 mm (3.9 in.) in increments of 5.08 mm (0.2 in.).

As seen in Figure 34, the stiffeners have a significant effect in lowering the SERR for the bending moment.

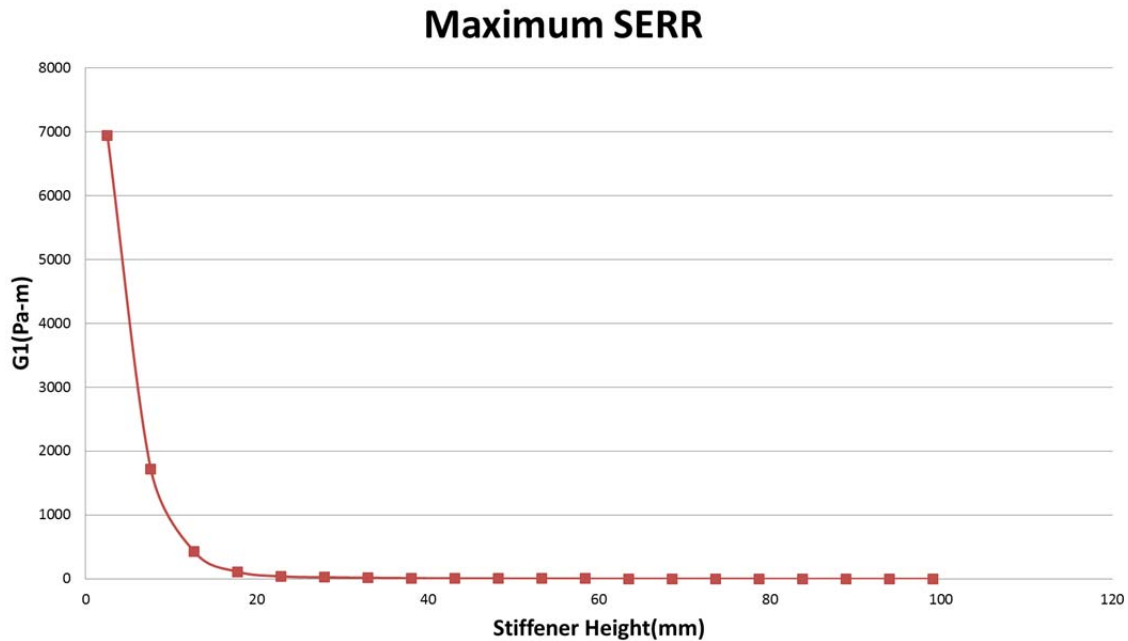


Figure 34 Maximum SERR for Varying Stiffener Height

As the stiffener height varies the SERR distribution across the thickness of the plate also changes. When the stiffener is small the maximum SERR occurs on the free side of the plate. When the stiffener height increases the SEER on the free side rapidly decreases until the maximum SERR is on the patched side. This can be seen in Figure 35.

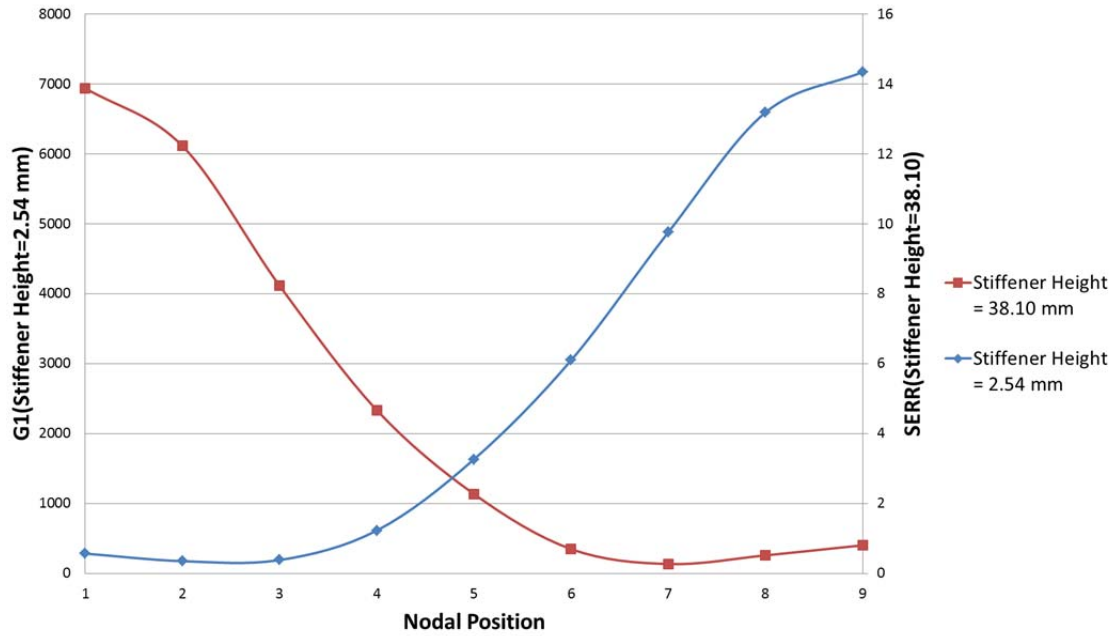


Figure 35 SERR Distribution

The change in the location of the maximum SERR can be explained by the location of the neutral axis. When the neutral axis is in the middle of the plate, as pictured top of Figure 36, the top of the plate is in compression and the bottom is in tension. As the stiffener height increases the neutral axis is lowered below the bottom of the plate. This causes the bottom of the plate to be in compression which closes the crack and reduces the SERR.

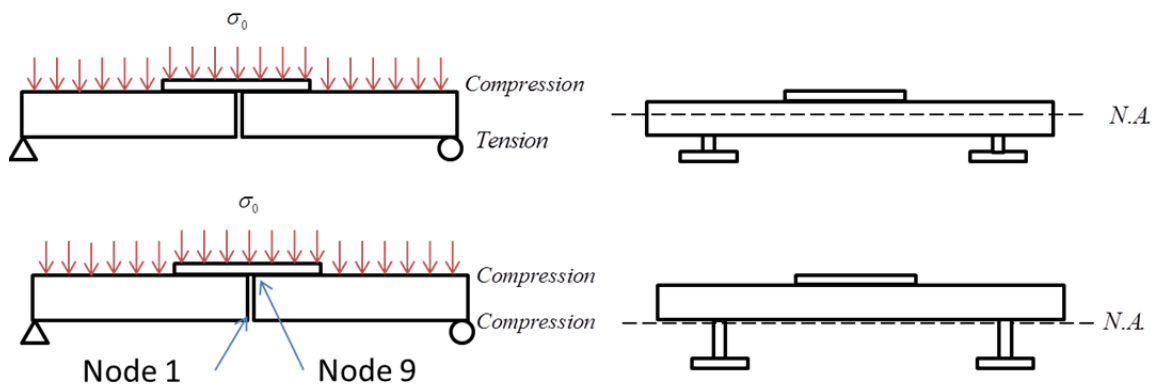


Figure 36 Neutral Axis Location for Bending Moment

2. Change in Plate Thickness

The second parameter considered for the bending moment was a change in the plate thickness. The thickness was varied from 3.81 mm (0.15 in.) to 8.89 mm (0.35 in.) in increments of 1.27 mm (0.05 in.). This was done for a plate with stiffener height of 25.4 mm (1 in.) and for various patch thickness and modulus of elasticity.

As seen in Figure 37, the SERR increases as the plate thickness is increased for the patched case and decreased for the unpatched case.

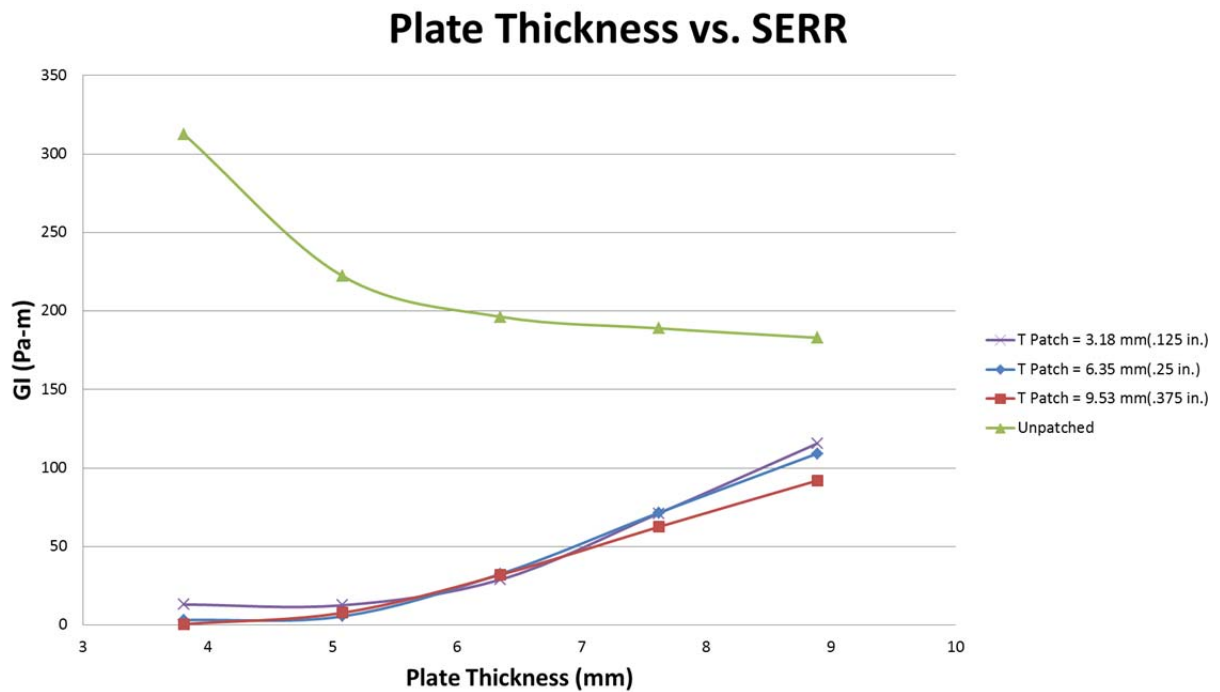


Figure 37 Various Plate Thicknesses while Applying a Bending Moment

This can be best explained by the location of the maximum SERR. Figure 38 illustrates the SERR distribution across the plate's thickness for the unpatched and patched plate. The SERR on the stiffener side is approximately the same for the patched and unpatched case. For the unpatched case the maximum SERR is on the opposite side of the stiffeners (node 9). For the patched case the maximum occurs on the same side of the stiffeners (node 1). As the thickness of the plate is increased the SERR increases on the stiffened side and decreased on the opposite side. This increases the maximum SERR

for the patched case and decreases it for the unpatched case. Figure 38 shows the SERR for two thicknesses; however this relation maintains the same for all thicknesses that were examined.

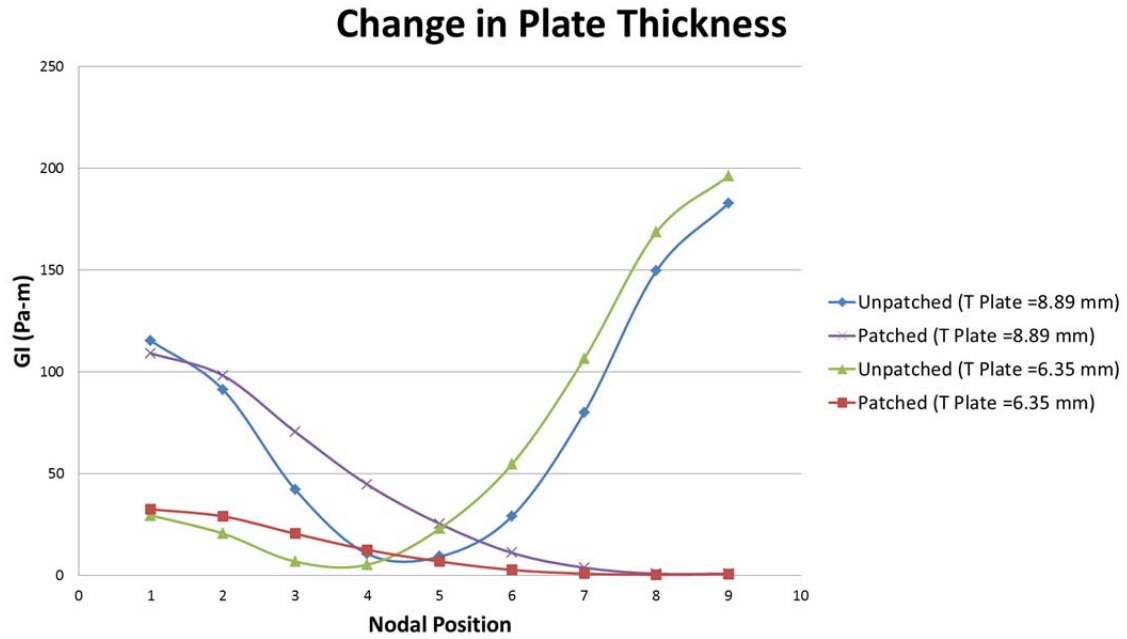


Figure 38 Location of Maximum SERR

V. CONCLUSIONS AND RECOMMENDATIONS

A. CONCLUSIONS

This study concluded that stiffener parameters and plate thickness have a significant effect on crack growth. This was determined to be true for both the tensile load and bending moment.

When applying a tensile load several important relations were found. First, a single-sided patch is more effective when applied to the opposite side rather than the same side of the plate as the stiffening members.

The location of the maximum SERR varied for different configurations. When a stiffening member is added, the SERR is decreased and the maximum SERR is shifted toward the unstiffened side. Whenever a patch is applied, the maximum SERR will be on the free side.

The location of the neutral axis is a vital component in predicting crack growth. Applying a patch to plate will cause the neutral axis to shift toward the patched side. The bending moment imposed by this shift can cause the patch to be ineffective and increase the SERR. This occurred when the properties of the patch are not stiff enough to cause the neutral axis to be raised above 63 percent of the plate's thickness. When this is the case, the patched model will experience more crack growth than the unpatched.

Lastly, an analytical model was developed that can be used to calculate the ratio of SERR for the patched and unpatched plate. This allows the effectiveness of the patch to be determined for a stiffened thick plate without the use of finite element software.

For the bending moment, the stiffener parameters and plate thickness still had a large influence on the SERR. Even when applying a small stiffener, the effect in reducing the SERR was significant. This was shown to lower the neutral axis below the bottom of the plate, causing it to switch from tension to compression and reduce the crack growth.

B. RECOMMENDATIONS

For future work it is recommended to compare the analytical and finite element results from this report with an experimental study. One of the difficulties for this experimental study would be choosing an appropriate method to attach the stiffeners to the plate. The most realistic method would be to weld them, using the same technique and settings used in naval construction. To make an accurate correlation between the numerical and experimental results, the residual stresses that are imposed on the plate from welding would have to be determined.

LIST OF REFERENCES

- [1] I. Grabovac and D. Whittaker, "Application of bonded composites in the repair of ships structures—A 15-year service experience," *Composites Part A: Applied Science and Manufacturing*, vol. 40, no. 9, pp. 1381–1398, 2009.
- [2] A. Baker, "Bonded composite repair of fatigue-cracked primary aircraft structures," *Composite Structures*, vol. 47, no. 1, pp. 431–443, 1999.
- [3] A. McGee, "Numerical study for optimum parameters of bonded composite repairs of cracked aluminum," M.S. thesis, Department Mechanical Engineering, Naval Postgraduate School, Monterey, CA, 2012. Available: <http://hdl.handle.net/10945/7384>
- [4] NSWC Carderock Division, Code 65, "U.S. Navy composite patch repair efforts for CG-46 class aluminum superstructures," unpublished
- [5] C. Wang, L. Rose, and R. Callinan, "Analysis of out-of-plane bending in one-sided bonded repair," *International Journal of Solids and Structures*, vol. 35, no. 14, pp. 1653–1675, 1998.
- [6] M. Belhouari, B. Bouiadjra, A. Megueni, and K. Kaddouri, "Comparison of double and single bonded repairs to symmetric composite structures; a numerical analysis," *Composite Structures*, vol. 65, no. 1, pp. 47–53, 2004.
- [7] A. Kumar and S. Hakeem, "Optimum design of symmetric composite patch repair to center cracked metallic sheet," *Composite Structures*, vol. 49, no. 3, pp. 285–292, 2000.
- [8] G.C. Tsai and S. B. Shen, "Fatigue analysis of cracked thick aluminum plate bonded with composite patches," *Composite Structures*, vol. 64, no. 1, pp. 79–90, 2004.
- [9] J. Klung and C. Sun, "Large deflection effects of cracked aluminum plates repaired with bonded composite patches," *Composite Structures*, vol. 42, pp. 291–296, 1998.
- [10] K. Madani, S. Touzain, X. Feaugas, M. Benguediab and M. Ratwani, "Numerical analysis for the determination of the stress intensity factors and crack opening displacements in plates repaired with single and double composite patches," *Computational Materials Science*, vol. 42, no. 3, pp. 385–393, 2008.

- [11] Y. Kwon, W. Lee, A. McGee, D. Hart, D. Loup and E. Rasmussen, “Analytical model for prediction of reduced strain energy release rate of single-side-patched plates,” *Applied Composite Materials*, vol. 20, no. 4, 2013.
- [12] C. Chue and T. Liu, “The effects of laminated composite patch with different stacking sequences on bonded repair,” *Composites Engineering*, vol. 5, no. 2, pp. 223–230, 1995.
- [13] S. Naboulsi and S. Mall, “Thermal effects on adhesively bonded composite repair of cracked aluminum panels,” *Theoretical and Applied Fracture Mechanics*, vol. 26, no. 1, pp. 1–12, 1997.
- [14] V. Sabelkin, S. Mall, M. Hansen, R. Vanawaker, and M. Derris, “Investigation into cracked aluminum plate repaired with Bonded composite patch,” *Composite Structures*, vol. 79, no. 1, pp. 55–66, 2007.
- [15] R. J. Dexter and P. J. Pilarski, “Effect of welded stiffeners on fatigue crack growth rate,” Ship Structure Committee, Washington, DC, Tech. Rep. CG-D-05–00, 2000.
- [16] S. Kou, *Welding Metallurgy, 2nd edition*, Hoboken: Wiley Interscience, 2003.
- [17] C. Poe, “Stress intensity factor for a cracked sheet with riveted and uniformly spaced stringers,” National Aeronautical and Space Administration, Washington, DC, Tech. Rep. TR-R-358, 1971.
- [18] V. Sabelkin S. Mall, and J.B. Avram, “Fatigue crack growth analysis of stiffened cracked panel repaired with bonded composite patch,” *Engineering Fracture Mechanics*, vol. 73, no. 1, pp. 1553–1567, 2006.
- [19] *ANSYS Mechanical APDL Contact Technology Guide*, Canonsburg, PA,: ANSYS Inc., 2012.
- [20] M. Meyers and K. Chawla, “Fracture: macroscopic aspects” *Mechanical Behavior of Materials*, Cambridge: Cambridge University Press, 2009, pp. 404–460.
- [21] R. Krueger, “Virtual crack closure technique: History, approach, and applications,” *Applied Mechanics Review*, vol. 57, no. 2, pp. 109–140, March 2004.
- [22] T. Anderson, *Fracture Mechanics: Fundamentals and Applications 2nd edition*, Boca Raton: CRC Press, 1995.
- [23] C. N. Duong and C. H. Wang, *Composite Repair: Theory and Design*, Oxford: Elsevier, 2007.

INITIAL DISTRIBUTION LIST

1. Defense Technical Information Center
Ft. Belvoir, Virginia
2. Dudley Knox Library
Naval Postgraduate School
Monterey, California